Preparation of Superhydrophobic Polypropylene / SiO_2 Coating for Self-Cleaning Application

Akshay R. Jundle[1], Rajaram S. Sutar[2], Rutuja A. Ekunde[1], Sagar S. Ingole[1], Pradip P. Gaikwad[1], Sanjay S. Latthe[1]*

[1] Self-cleaning Research Laboratory, Department of Physics, Vivekanand College, Kolhapur (An Empowered Autonomous Institute), (Affiliated to Shivaji University, Kolhapur), Kolhapur – 416003, Maharashtra, India.

[2] School of Chemistry and Molecular Sciences, Henan University, Kaifeng, China.

*Corresponding author E-mail: latthes@gmail.com

Abstract

This study introduces a straightforward and cost-efficient dip-coating technique for the fabrication of hierarchical superhydrophobic nanocomposite coatings. Hydrophobic silica nanoparticles (NPs) were synthesized via the sol–gel method and subsequently integrated into a polypropylene matrix. The degree of superhydrophobicity was adjusted by varying the concentration of silica NPs within the polymer solution. Upon optimization, the coating achieved a water contact angle (WCA) of 165° and a sliding angle of 7°. Surface morphological analysis revealed a hierarchical rough structure on the coated glass substrate, which facilitated air entrapment and contributed to the observed water-repellent behavior. The coating demonstrated excellent wetting stability under water jet impact and exhibited notable self-cleaning characteristics. Mechanical durability was assessed through sandpaper abrasion and adhesive tape peeling tests, confirming the coating's robustness. These highly non-wettable and self-cleaning surfaces hold promise for a range of practical applications.

Keywords: Superhydrophobic, Self-cleaning, Nanocomposite, Coatings, Glass

Introduction

In recent years, the development of superhydrophobic surfaces has garnered significant attention from both scientific and industrial communities due to their remarkable water-repellent **[1]**, self-cleaning **[2]**, anti-fouling **[3]**, and anti-corrosive **[4]** properties. A surface is deemed superhydrophobic when its static WCA exceeds 150°, and the sliding angle (SA) is less than 10°, allowing water droplets to bead and roll off easily, thereby removing contaminants. This self-cleaning effect is inspired by natural surfaces such as lotus leaves and butterfly wings, which exhibit hierarchical surface roughness combined with low surface energy materials, resulting in minimal solid–liquid contact **[5]**. The application of this principle in engineered coatings has led to advancements in fields such as construction materials, textiles, solar panels, marine applications, and biomedical devices.

Among various polymeric materials, polypropylene (PP) has emerged as a promising matrix for superhydrophobic coatings due to its inherent hydrophobicity, excellent chemical resistance, low density, and thermal stability **[6]**. However, pristine polypropylene lacks the surface roughness and surface energy manipulation required to achieve true superhydrophobicity. Therefore, modifying polypropylene by incorporating nanostructured fillers such as silicon dioxide (SiO_2) and optimizing surface morphology becomes essential[6]. SiO_2 nanoparticles are particularly advantageous for this purpose due to their high surface area, tunable size, chemical stability, and ability to form micro/nano hierarchical textures on polymer surfaces. Several strategies have been reported for fabricating superhydrophobic polymer/inorganic composite coatings, including sol–gel synthesis **[7]**, spray coating **[8]**, dip coating **[9]**, and phase separation methods **[10]**. These approaches generally involve creating multi-scale roughness and reducing surface

energy by employing fluorinated or silane-based functional groups. However, challenges persist in ensuring uniform dispersion of nanoparticles, maintaining mechanical durability, and achieving scalable, environmentally friendly fabrication processes. Moreover, the integration of low-cost polymers like polypropylene with functional inorganic components such as SiO_2 opens new avenues for industrially viable, high-performance self-cleaning surfaces **[11]**. The synergistic combination of polypropylene and SiO_2 nanoparticles can provide a dual-functional system: the hydrophobic polypropylene serves as the base matrix to enhance chemical stability and weather resistance, while the SiO_2 nanoparticles introduce hierarchical surface roughness essential for water droplet mobility.

By tailoring the dispersion of SiO_2 in the polymer matrix and optimizing the coating process, it is possible to fabricate robust, superhydrophobic surfaces suitable for real-world applications. This study aims to develop a superhydrophobic PP/SiO_2 composite coating via a facile spray-coating method for self-cleaning applications. The research focuses on optimizing the concentration of SiO_2 nanoparticles and evaluating their effect on surface wettability, morphology, and durability. Comprehensive characterization of the prepared coatings is performed using contact angle measurements. Ochir et al. **[12]** successfully engineered a durable superhydrophobic surface by applying a coating of hydrophobic silica nanoparticles (SNPs) onto polypropylene (PP) through a straightforward compression molding technique. The resultant coating exhibited a high WCA of approximately 170° and a low sliding angle of less than 5°, attributed to its nano/microscale roughness and low surface energy. The coating demonstrated remarkable mechanical durability, maintaining its superhydrophobic properties after enduring 25 tape peel cycles and 100 cm sandpaper scratch tests. Additionally, it exhibited good chemical stability in acidic and neutral environments, although it was less stable under alkaline conditions. This method presents a scalable and cost-effective strategy for fabricating robust, self-cleaning superhydrophobic surfaces, making it suitable for practical applications. Moradi et al. **[11]**developed a superhydrophobic and anti-corrosion polypropylene (PP) coating for mild steel surfaces by incorporating polypropylene grafted with maleic anhydride (PP-g-MAH) and graphene oxide (GO) into the PP matrix. These additives significantly enhanced the coating's compactness, corrosion resistance, and hydrophobicity. The optimal formulation, consisting of 1.5 g PP-g-MAH and 2 mg GO, achieved a contact angle of 166°, a surface roughness of 87 nm, and corrosion resistance 800 times greater than that of pure PP. Molecular dynamics (MD) simulations further confirmed an increase in coating density from 0.80 to 0.85 g/cm³ due to the presence of GO. After immersion in NaCl solution for 2 hours, the coating with 2 mg GO maintained superior corrosion resistance, demonstrating its effectiveness in protecting construction metals such as mild steel.

In this study, hydrophobic silica NPs were synthesized using the sol–gel method with methyltrimethoxysilane (MTMS) serving as the precursor. A suspension containing the synthesized silica NPs and polypropylene was applied to glass substrates through a controlled dip-coating process, which involved regulated dipping and withdrawal speeds. The resultant coating demonstrated excellent self-cleaning properties, as evidenced by a high WCA of 165°, allowing water droplets to roll off the surface effortlessly.

Experimental section

Materials

Sigma-Aldrich (USA) provided Methyltrimethoxysilane (MTMS, 98%) and Polypropylene Changshu Hongsheng Fine Chemical Co., Ltd. (China) supplied Ethanol (99.9%). Ammonium hydroxide (MW 35.05) has been provided by Research Lab Pvt. Ltd. (Mumbai, India). Micro-glass slides (75 × 25 × 1.35 mm) were obtained from Blue star, Polar Industrial Corporation, India.

Synthesis of Hydrophobic Silica Nanoparticles

Hydrophobic silica nanoparticles were synthesized using the sol–gel method, employing methyltrimethoxysilane (MTMS) as the silica precursor. In a typical synthesis, 4 mL of MTMS was combined with 40 mL of methanol and 8 mL of deionized water. The resulting solution was stirred with a magnetic stirrer for 20 minutes at room temperature to initiate the hydrolysis process. Subsequently, ammonium hydroxide solution, serving as a catalyst, was added dropwise to the mixture under continuous stirring. The reaction was allowed to proceed for an additional 30 minutes to facilitate condensation and gelation. The resulting gel was aged at room temperature overnight to enhance the structural integrity of the silica network. Following aging, the gel was dried in an oven at 80 °C for 5 hours to remove residual solvents and moisture. The dried xerogel was then mechanically ground using a mortar and pestle to obtain fine, nanoscale silica particles suitable for further use.

Preparation of Polypropylene/Silica Nanocomposite Coating

To prepare the superhydrophobic coating, 10 mg of polypropylene (PP) granules were dissolved in 10 mL of o-xylene under magnetic stirring for 30 minutes to ensure complete dissolution of the polymer. Subsequently, 150 mg of the previously synthesized hydrophobic silica nanoparticles were added to the polymer solution, and the mixture was subjected to ultrasonication in an ultrasonic cleaner for 20 minutes to promote uniform nanoparticle dispersion. Glass substrates were cleaned and then dip-coated in the prepared PP/SiO_2 nanocomposite solution. Each substrate was immersed for 6 seconds per cycle, and the dip-coating process was repeated for a total of 10 cycles to achieve adequate coating thickness and surface uniformity. The coated substrates were subsequently dried in a hot air oven at 120 °C for 3–4 hours to ensure solvent evaporation and proper film formation.

Characterizations

WCA and WSA were determined using a contact angle goniometer (HO-IAD CAM-01, Holmarc Opto-Mechatronics Pvt. Ltd., India). To ascertain the roll-off angle, the coated glass substrate was affixed to the instrument's sample holder, which was incrementally inclined using an adjustment screw until the droplet commenced rolling off. For the water jet impact test, a continuous stream of water was applied to the coating via a 15 mL syringe. Furthermore, water droplets were released from a height of approximately 10 cm onto the coating surface, inclined at an angle of 30°, to evaluate dynamic wettability. The mechanical durability of the coating was assessed through adhesive tape peeling, sandpaper abrasion, and sand gran impact tests. Self-cleaning performance was evaluated by dispersing artificial dust particles onto the coated surface, followed by observing the removal behavior under water flow.

Results and discussion

The synthesis of hydrophobic silica nanoparticles (SNPs) via the sol–gel method using methyltrimethoxysilane (MTMS) as the organosilane precursor is a well-established approach for producing functionalized nanomaterials with tunable surface properties. MTMS, a trifunctional silane, provides both the silica source and hydrophobic methyl groups, which are crucial for tailoring the surface energy of the resulting nanoparticles. The initial mixing of MTMS, methanol, and deionized water, followed by stirring at room temperature, facilitates the hydrolysis of methoxy groups on MTMS to form silanol groups (–Si–OH). This reaction is essential as it governs the extent and uniformity of network formation. Methanol acts as a solvent and homogenizing agent, while water serves as the reactant for hydrolysis. The dropwise addition of

ammonium hydroxide introduces a basic environment that catalyzes the condensation of silanol groups, leading to the formation of a three-dimensional silica network through siloxane (Si–O–Si) bonds. The controlled addition and continuous stirring help in regulating nucleation and growth processes, resulting in uniform nanoparticle formation. The subsequent aging step, performed overnight at ambient conditions, is critical for network rearrangement and strengthening of the gel, contributing to improved porosity and mechanical integrity of the silica matrix.

Drying the gel at 80 °C removes volatile components, transitioning the gel into a xerogel. This step must be carefully controlled to avoid pore collapse, ensuring retention of the nanoscale porosity. Mechanical grinding of the dried xerogel breaks down the bulk structure into fine particles, yielding nanoscale hydrophobic silica with a large specific surface area and suitable surface chemistry for functional applications.

Wettability and self-cleaning ability

The wettability of a solid surface is largely determined by its chemical composition and surface morphology. In this study, coating performance was evaluated by varying the number of dipping cycles—specifically 8, 9, and 10 cycles—resulting in samples labeled P1, P2, and P3, respectively. The P1 sample exhibited a WCA of 145° with a low sliding angle (SA) of 9°, indicating hydrophobic behavior. The P2 sample demonstrated improved performance, with a WCA of 151° and a reduced SA of 7°, suggesting enhanced water repellency.

As shown in Figure 1a, the S3 sample displayed nearly spherical water droplets, corresponding to a high WCA of approximately 165° (Figure 1b). The slight difference of only 3° between the left and right contact angles indicates excellent surface uniformity. Water droplets rolled off the surface with ease, supported by the low SA of 7°, confirming the strong non-wetting, superhydrophobic character of the P3 coating. This superior performance is attributed to the rough and porous surface morphology of the coating. This confirms that the silica nanoparticles–polypropylene nanocomposite was uniformly deposited, forming a consistently rough and porous structure across the substrate.

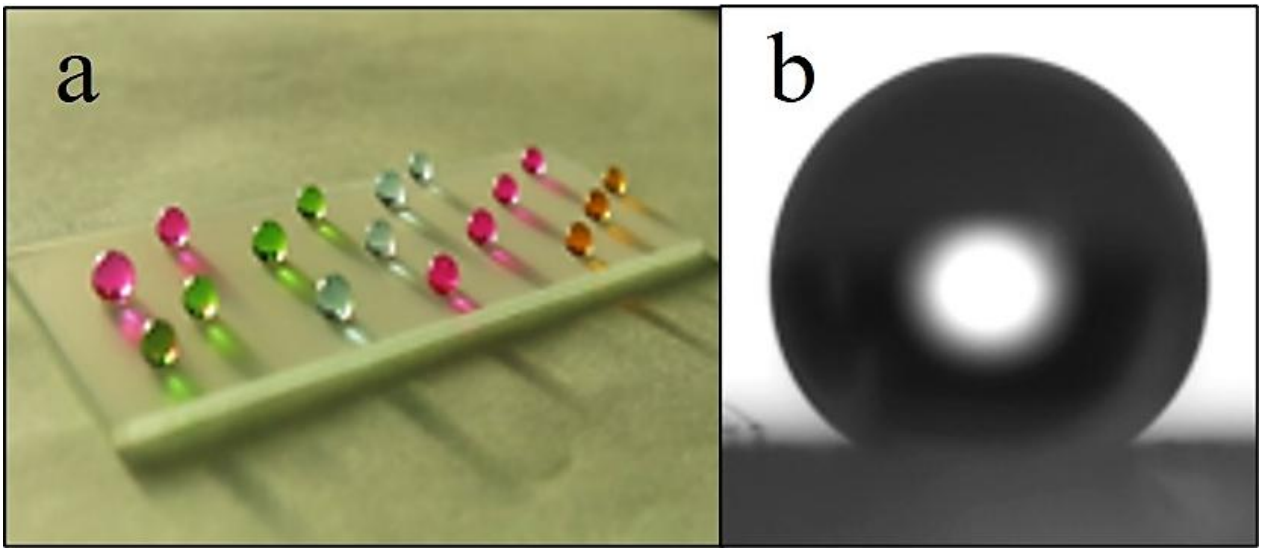

Figure 1. (a) The optical photographs of the colored water droplets on the P3 sample. **(b)** WCA image on the P3 sample.

The images shown demonstrate the self-cleaning behavior of a superhydrophobic coating applied to a glass substrate. In image (a), the surface is intentionally soiled with fine dust or soil particles. In image (b), a stream of water is gently poured onto the coated surface. As observed, the water droplet rolls down the

inclined surface, carrying the soil particles away with it. This clearly indicates that the surface exhibits excellent self-cleaning properties, where the low surface energy and micro/nano-structured roughness prevent the adhesion of contaminants. Instead, the dirt is picked up and removed by rolling water droplets, confirming the effectiveness of the superhydrophobic coating in maintaining a clean surface with minimal effort.

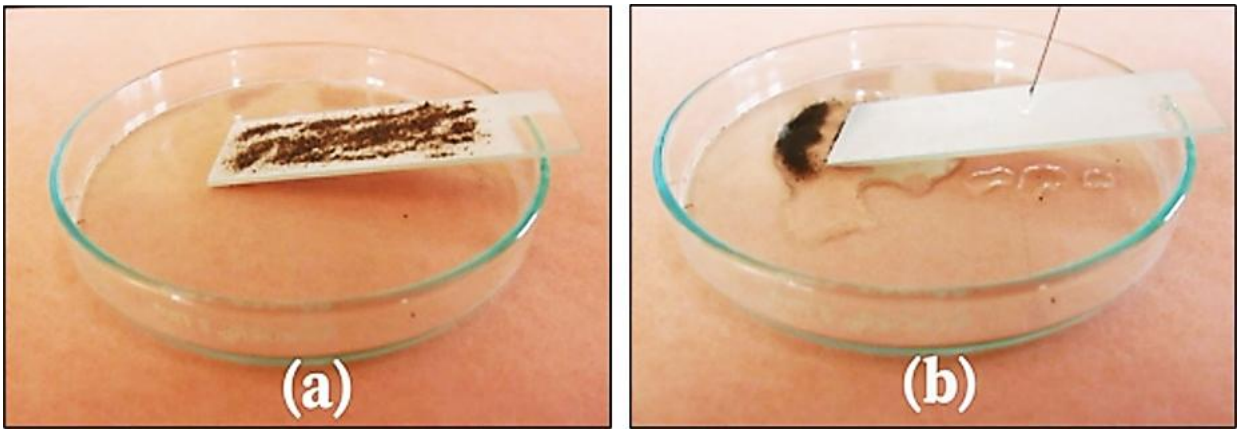

Figure 2. (a) The optical photographs of the soil particles spread on the P3 sample, **(b)** soil particles washed away easily by the rolling water droplets.

Mechanical durability of the coating

The mechanical durability of the superhydrophobic coating was inspected by adhesive tape, sandpaper abrasion test, and sand grain impact. The adhesive and mechanical durability of the superhydrophobic P3 coating was evaluated through adhesive tape peeling and sandpaper abrasion tests. In the tape peeling test, an adhesive tape was gently pressed onto the coated surface and slowly peeled off to assess the coating's adhesion strength. The coating retained its superhydrophobic nature for up to one peeling cycle. However, after the second cycle, the WCA dropped to 139°, indicating partial removal of the nanocomposite layer. With subsequent cycles, the WCA continued to decline, reflecting poor adhesion, and by the sixth cycle, the coating became hydrophilic with a WCA of 56° (Figure 3a).

The mechanical robustness was further assessed using the sandpaper abrasion test. Here, the P3-coated surface was placed face-down on 400-grit sandpaper under a 20 g load and moved across a 10 cm distance per cycle. The coating maintained superhydrophobicity up to two abrasion cycles. Beyond this point, the WCA declined sharply, signifying the progressive erosion of the nanocomposite layer caused by mechanical abrasion. After 50 abrasion cycles, the coating was completely removed, leaving a hydrophilic surface with a WCA of 68°, as illustrated in Figure 3b. These results highlight the coating’s limited mechanical durability and adhesion strength under repeated physical stress.

To evaluate the mechanical durability of the coating under simulated sandstorm conditions, a series of sand impact tests were conducted on the P3 marble sample. In each cycle, 10 g of sand was dropped from a height of 20 cm above the sample, totaling 30 g over three cycles. As depicted in Figure 3c, the WCA progressively decreased with increasing impact cycles. Following three sand impact cycles, the coating exhibited a significant reduction in WCA to approximately 46°, indicating moderate resistance to mechanical wear under simulated sandstorm conditions.

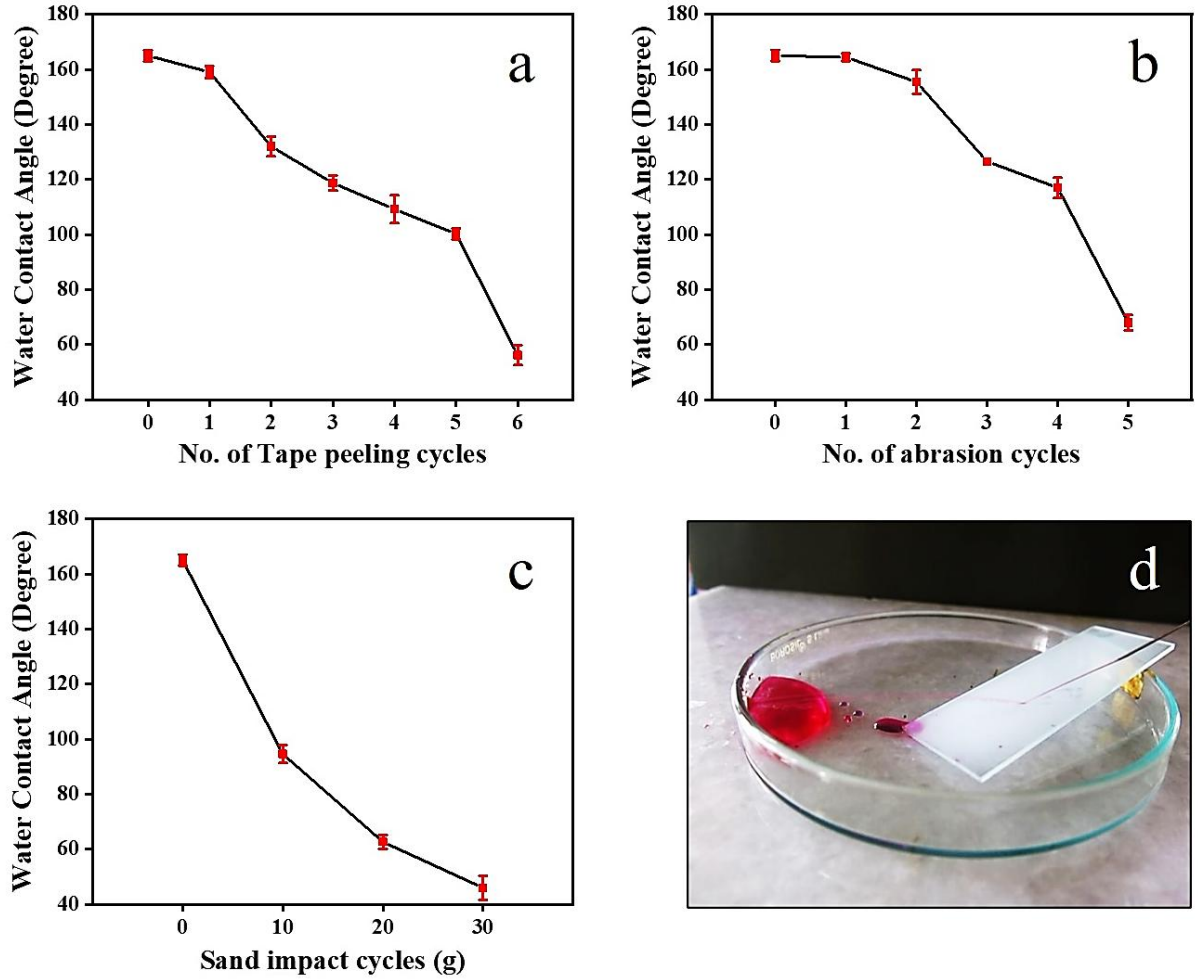

Figure 3. (a) Variation in WCA after each adhesive tape cycle, **(b)** variation in WCA after each sandpaper abrasion cycle, **(c)** variation in WCA after 10 g of sand gran impacting, **(d)** optical photograph of P3 sample repelling water jet.

A water jet generated from a syringe was directed onto the coated glass substrate. Upon striking the SHP P3 sample, the water jet bounced off the surface, indicating its strong water-repellent nature, as illustrated in Figure 3(d). This behavior can be attributed to the hierarchical surface structure, which traps air pockets and prevents water penetration into the coating. The water jet was continuously applied to a fixed point on the surface for over 2 minutes, and the persistent rebounding of the jet confirmed the excellent mechanical robustness and durability of the P3 coating.

Conclusions

In conclusion, a superhydrophobic coating was effectively developed on glass substrates by applying a layer of polypropylene and silica nanoparticles using a dip-coating method. The resultant coated surface demonstrated exceptional water-repellent characteristics, with a WCA of 165° and a water sliding angle (WSA) of 7°. In terms of durability, the coating exhibited significant mechanical resilience, maintaining its superhydrophobic properties after undergoing one cycle each of adhesive tape peeling and sandpaper abrasion, as well as after exposure to 10 g of sand impact and prolonged water jet testing.

Acknowledgements

One of the authors, SSL, is grateful for financial assistance received through the Seed Money Scheme from Vivekanand College, Kolhapur (Empowered Autonomous), Ref. No. VCK/3108/2023-24 dated 30/03/2024.

References

[1] S. Long, Y. Hu, X. Dong, L. Shen, Y. Wang, Y. Huang, X. Li, Superhydrophobic Polypropylene Surface via Migration of SiO2 Nanoparticles with Low Surface Energy, Macromolecular Rapid Communications, (2025) 2500195.

[2] S. Man, L. Yang, X. Fan, J. Chen, Z. Shi, M. Zhang, M. Li, Hierarchical PVA/SiO_2 hybrid coating constructs superhydrophilic/underwater superoleophobic polypropylene membranes for efficient emulsion separation, Journal of Water Process Engineering, 73 (2025) 107762.

[3] M.-C. Han, S.-Z. Cai, J. Wang, H.-W. He, Single-side superhydrophobicity in Si3N4-doped and SiO2-treated polypropylene nonwoven webs with antibacterial activity, Polymers, 14 (2022) 2952.

[4] A. Ansari, N.M. Nouri, A one step self-cleaning surface with robust superhydrophobic and photocatalytic properties: Electrostatic sprayed fluorinated ethylene propylene mixed with nano TiO2–SiO2 particles, Ceramics International, 49 (2023) 57-66.

[5] N. Kanovsky, T. Iline-Vul, S. Margel, In-situ design of hierarchical durable silica-based coatings on polypropylene films with superhydrophilic, superhydrophobic and self-cleaning properties, Results in Surfaces and Interfaces, 10 (2023) 100101.

[6] Y. Liu, Z. Zhao, Y. Shao, Y. Wang, B. Liu, Preparation of a superhydrophobic coating based on polysiloxane modified SiO2 and study on its anti-icing performance, Surface and Coatings Technology, 437 (2022) 128359.

[7] Y. Wang, S. Ge-Zhang, P. Mu, X. Wang, S. Li, L. Qiao, H. Mu, Advances in sol-gel-based superhydrophobic coatings for wood: a review, International Journal of Molecular Sciences, 24 (2023) 9675.

[8] H. Daneshmand, A. Sazgar, M. Araghchi, Fabrication of robust and versatile superhydrophobic coating by two-step spray method: An experimental and molecular dynamics simulation study, Applied Surface Science, 567 (2021) 150825.

[9] Q. Wang, G. Sun, Q. Tong, W. Yang, W. Hao, Fluorine-free superhydrophobic coatings from polydimethylsiloxane for sustainable chemical engineering: Preparation methods and applications, Chemical Engineering Journal, 426 (2021) 130829.

[10] R. Zhang, J. Wei, N. Tian, W. Liang, J. Zhang, Facile preparation of robust superamphiphobic coatings on complex substrates via nonsolvent-induced phase separation, ACS Applied Materials & Interfaces, 14 (2022) 49047-49058.

[11] M. Moradi, M. Rezaei, Construction of highly anti-corrosion and super-hydrophobic polypropylene/graphene oxide nanocomposite coatings on carbon steel: Experimental, electrochemical and molecular dynamics studies, Construction and Building Materials, 317 (2022) 126136.

Synthesis and Structural Characterization of Nickel Ferrite ($NiFe_2O_4$) Nanoparticles via Sol-Gel Auto-Combustion Method

Dhiraj P. Bhingardeve1, Avinash R. Gaikwad1
1 Department of Physics, Vivekanand College, Kolhapur
(An Empowered Autonomous Institute), (Affiliated to Shivaji University, Kolhapur),
Kolhapur – 416003, Maharashtra, India.
*Corresponding author E-mail: argphysics@gmail.com

Abstract

Nickel ferrite ($NiFe_2O_4$) nanoparticles were successfully synthesized using the sol-gel auto-combustion method. This technique offers a cost-effective, low-temperature route to obtain phase-pure spinel ferrite with nanocrystalline morphology. Citric acid was used as a chelating and fuel agent, and the pH was adjusted using ammonia. The obtained powder was calcined at 600 °C and analyzed using X-ray diffraction (XRD). The XRD pattern confirmed the formation of a single-phase cubic spinel structure without detectable impurity peaks. The average crystallite size, calculated using the Debye–Scherrer formula, was found to be in the range of 20–30 nm. The results demonstrate that the sol-gel auto-combustion method is suitable for producing high-purity $NiFe_2O_4$ nanoparticles for magnetic, sensor, and catalytic applications.

Keywords: Nickel ferrite, Sol-gel auto-combustion, Spinel structure, Nanoparticles

1. Introduction

Spinel ferrites with the general formula MFe_2O_4, where M represents a divalent metal ion such as Ni^{2+}, Co^{2+}, or Zn^{2+}, have garnered significant attention due to their remarkable structural stability, moderate electrical conductivity, and excellent magnetic properties [1, 2]. Among these, nickel ferrite ($NiFe_2O_4$) is an inverse spinel where Ni^{2+} ions predominantly occupy the octahedral sites, while Fe^{3+} ions are distributed between tetrahedral and octahedral sites, leading to intriguing magnetic and electrical behavior [3]. Because of these properties, $NiFe_2O_4$ is widely utilized in magnetic recording media, microwave devices, catalysis, biomedical applications, and gas sensing [4, 5]. The performance of ferrite materials is highly dependent on their synthesis method, which influences properties such as particle size, morphology, crystallinity, and magnetic behavior. Traditional ceramic methods often require high sintering temperatures and extended processing times, which can lead to grain growth and inhomogeneity [6]. In contrast, wet chemical routes like the sol-gel auto-combustion method offer precise stoichiometric control, low processing temperatures, and uniform particle distribution at the nanoscale [7]. In the sol-gel auto-combustion process, metal nitrates are chelated with organic fuels such as citric acid. Upon drying and ignition, the gel undergoes a self-sustained exothermic reaction, leading to the formation of ferrite powder with nanocrystalline features. This method also facilitates homogenous mixing at the molecular level, ensuring better phase purity and fine particle sizes.

In this study, we report the successful synthesis of $NiFe_2O_4$ nanoparticles via the sol-gel auto-combustion method. The structural properties of the synthesized ferrite were examined using X-ray diffraction (XRD) to confirm phase purity, crystallite size, and lattice parameters. The objective is to demonstrate the suitability of this method for producing high-quality $NiFe_2O_4$ for potential use in advanced magnetic and electronic applications.

2. Experimental Method

2.1 Materials

All chemicals used in this study were of analytical grade and used without further purification. Nickel nitrate hexahydrate ($Ni(NO_3)_2 \cdot 6H_2O$), ferric nitrate nonahydrate ($Fe(NO_3)_3 \cdot 9H_2O$), and citric acid monohydrate ($C_6H_8O_7 \cdot H_2O$) were procured from Sigma-Aldrich and used as starting materials. Deionized water was used throughout the synthesis.

2.2 Synthesis of $NiFe_2O_4$ Nanoparticles

Nickel ferrite nanoparticles were synthesized via the sol-gel auto-combustion method [8]. Schematic diagram shown in Figure 1. Stoichiometric amounts of nickel nitrate and ferric nitrate (molar ratio 1:2) were dissolved in deionized water under constant stirring. Citric acid was added to the metal nitrate solution as a chelating agent, maintaining a metal nitrates to citric acid molar ratio of 1:1 [9, 10]. The resulting solution was stirred continuously at 80°C to obtain a homogeneous sol. As water evaporated, the sol gradually transformed into a viscous gel. The gel was then heated on a hot plate at ~200°C to initiate the auto-combustion reaction. The exothermic nature of the reaction resulted in the spontaneous ignition of the gel, producing a voluminous, fluffy black powder, indicative of the formation of nickel ferrite [11].

2.3 Calcination

The as-combusted powder was ground using an agate mortar and pestle and then calcined in a muffle furnace at 600°C for 4 hours to improve crystallinity and remove any residual organic matter [12]. The heating rate was maintained at 5°C/min to avoid thermal shocks. After calcination, the powder was cooled naturally to room temperature and stored in airtight containers for further characterization.

2.4 Material Characterizations:

The powder approach is frequently used to facilitate the crystal structure investigation of a material easier. A continuous spectrum of X-rays with a fixed angle of incidence is used in the Laue method, one of the first techniques used for identifying crystal structure [16]. This technique is appropriate for detecting dynamic processes inside the crystal structure because it yields diffraction conclusions more quickly than those obtained with monochromatic X-rays. This method is called the centered crystal method when the wavelength varies but the angle of incidence remains fixed. The sample in this procedure rotates at a fixed angular velocity and is exposed to a monochromatic hard X-ray beam. On the other hand, the angle of incidence varies while the wavelength remains constant with the powder approach. Calculating crystal dimensions with the Scherrer equation is an essential use of XRD in nanocrystal studies [13].

where, β is full width at half maximum (FWHM) of the diffraction peak, and θ is the peak position in radians.

In this work, XRD confirmed the formation of single-phase spinel $NiFe_2O_4$ with good crystallinity. No impurity peaks were observed, indicating high phase purity. The crystallite size was found to be in the nanometer range, consistent with the nature of the sol-gel auto-combustion synthesis process.

3. Results and Discussions:

3.1 Reaction Mechanism for the Sol-Gel Auto-Combustion Synthesis of $NiFe_2O_4$:

The sol-gel auto-combustion method is a versatile chemical synthesis route used to prepare homogeneous and phase-pure nanocrystalline materials at relatively low temperatures. In this process, metal nitrates act as oxidizers while a suitable organic fuel (typically citric acid or glycine) serves as the reducing agent and complexing agent. The process involves three key steps: (i) sol formation, (ii) gelation, and (iii) auto-combustion. In this study, nickel nitrate [$Ni(NO_3)_2 \cdot 6H_2O$] and ferric nitrate [$Fe(NO_3)_3 \cdot 9H_2O$] were used as the metal precursors, while citric acid ($C_6H_8O_7$) served as both the complexing agent and fuel. The molar ratio of metal ions to citric acid was carefully optimized (typically 1:1 or 1:2) to ensure stoichiometry and efficient combustion.

Step 1: Complexation and Sol Formation

Upon dissolving the metal nitrates and citric acid in deionized water under constant stirring, complexation occurs through the chelation of metal cations by citric acid. This leads to the formation of a homogeneous sol containing metal–citrate complexes in eq.2.

$$Ni2+ + Fe3+ + C6H8O7 \rightarrow [Ni\text{-}Citrate\text{-}Fe]complex + H+ \quad \ldots (2)$$

The citric acid acts by binding through its carboxylate and hydroxyl groups, stabilizing the metal ions in solution and preventing precipitation [14].

Step 2: Gelation

On heating (around 70–90°C), the sol gradually loses water and becomes more viscous, forming a gel-like structure. This gel contains uniformly distributed metal ions embedded in an organic matrix in eq. 3.

$$[Ni\text{-}Citrate\text{-}Fe]complex \rightarrow Polymeric\ Gel \quad \ldots (3)$$

This gelation process is vital to ensure uniform distribution of cations, which ultimately results in homogeneous particle size upon combustion [15].

Step 3: Auto-Combustion Reaction

On further heating (around 150–250°C), the dried gel undergoes a self-sustained exothermic combustion reaction due to the redox interaction between the oxidizing nitrates and the reducing citric acid. This results in the rapid release of gases such as CO_2, H_2O, and N_2, and the formation of a voluminous, fluffy, and porous powder in eq. 4.

$$C6H8O7 + NO3^- \rightarrow NiFe2O4 + CO2 + H2O + N2 + Heat \quad \ldots (4)$$

The approximate redox-based combustion reaction can be written as eq. 5.

$$Ni(NO3)2 + 2Fe(NO3)3 + C6H8O7 \rightarrow NiFe2O4 + 6NO2 + 6H2O + 6CO2 \quad \ldots (5)$$

The combustion is self-propagating and provides the thermal energy necessary for in-situ crystallization of the spinel ferrite phase. No external calcination may be required if the combustion is sufficiently exothermic.

Crystallization of $NiFe_2O_4$ Spinel Phase:

The final product is nanocrystalline nickel ferrite ($NiFe_2O_4$), which crystallizes in the cubic spinel structure (space group $Fd\bar{3}m$), with Ni^{2+} occupying the octahedral (B) sites and Fe^{3+} distributed between tetrahedral (A) and octahedral sites in eq. 6 [16].

$$Ni2+ + 2Fe3+ + 4O2^- \rightarrow NiFe2O4 \quad \ldots (6)$$

3.2 X-ray Diffraction (XRD) Analysis

The phase purity and crystalline structure of the synthesized $NiFe_2O_4$ nanoparticles were characterized using X-ray diffraction (XRD) in the 2θ range of 10°–80° in Figure 1. The diffraction peaks observed at 2θ values approximately 30.2°, 35.6°, 43.3°, 53.6°, 57.2°, and 62.9° correspond to the (220), (311), (400), (422), (511), and (440) crystal planes, respectively. These reflections are well indexed to the face-centered cubic (FCC) spinel structure of nickel ferrite ($NiFe_2O_4$) and are in good agreement with the standard JCPDS card no. 10-0325 [17, 18]. The most intense peak at 35.6°, assigned to the (311) plane, confirms the formation of a single-phase spinel ferrite. No additional peaks corresponding to impurities or secondary phases such as NiO or Fe_2O_3 were detected, indicating the phase purity of the synthesized material [19]. The sharp and well-defined nature of the peaks suggests that the material is crystalline, while the moderate broadening indicates the nanoscale size of the crystallites. The formation of a spinel structure can be attributed to the homogeneous mixing of metal precursors and the rapid combustion process that promotes uniform nucleation and growth of nanoparticles during synthesis. These structural features make $NiFe_2O_4$ a promising candidate for applications in magnetic materials, microwave devices, and supercapacitors [20].

Fig. 1: X-ray diffraction pattern of NiFe2O4 annealed at 600□ C for 2 h.

3. Conclusions

In this study, nickel ferrite ($NiFe_2O_4$) nanoparticles were successfully synthesized using the sol-gel auto-combustion method. The X-ray diffraction (XRD) analysis confirmed the formation of a single-phase spinel structure with high crystallinity. The average crystallite size, calculated using the Scherrer equation, was found to be in the nanometer range, indicating the effectiveness of the sol-gel process in controlling particle growth. The sharp and intense diffraction peaks further suggest good crystallinity and phase purity of the synthesized material. The sol-gel auto-combustion method proved to be a cost-effective, energy-efficient, and facile route for producing $NiFe_2O_4$ nanoparticles with controlled morphology and desirable structural properties. These results suggest that $NiFe_2O_4$ synthesized by this method holds potential for applications in magnetic devices, sensors, and energy storage systems. Future studies may focus on detailed magnetic, electrical, and electrochemical investigations to explore its practical applications in various technological fields.

4. References

1) Goldman, A. (2006). Modern Ferrite Technology. Springer.

2) Kodama, R. H. (1999). Magnetic nanoparticles. Journal of Magnetism and Magnetic Materials, 200(1-3), 359–372.

3) Ghasemi, A., et al. (2008). Nanocrystalline $NiFe_2O_4$ ferrite prepared by sol–gel auto-combustion method. Journal of Alloys and Compounds, 465(1-2), 387–391.

4) Mahmood, T., et al. (2013). Structural and magnetic properties of $NiFe_2O_4$ nanoparticles prepared by a low-temperature solution combustion method. Journal of Magnetism and Magnetic Materials, 330, 138–142.

5) Ahmed, M. A., et al. (2010). Structural and magnetic properties of nanocrystalline $NiFe_2O_4$ ferrite. Materials Chemistry and Physics, 123(1), 118–123.

6) Gul, I. H., et al. (2008). Structural, magnetic and electrical properties of cobalt ferrites synthesized by co-precipitation route. Journal of Magnetism and Magnetic Materials, 320(3-4), 270–275.

7) Sayyed, M. I., et al. (2020). Ni–Mg ferrite as a potential gamma-ray shielding material: synthesis, characterization and radiation attenuation study. Journal of Materials Science: Materials in Electronics, 31(12), 9708–9720.

8) Rani, S., et al. (2019). Synthesis and characterization of Ni-Mg ferrite nanoparticles for gas sensing applications. Journal of Materials Science: Materials in Electronics, 30(11), 10661–10670.

9) Arulmurugan, R., et al. (2005). Magnetic and dielectric behavior of nanocrystalline Ni–Zn and Ni–Cu ferrites synthesized by co-precipitation method. Journal of Magnetism and Magnetic Materials, 288, 470–477.

10) Sundararajan, M., et al. (2014). Effect of Mg substitution on the structure and magnetic properties of nickel ferrite nanoparticles synthesized by sol-gel method. Ceramics International, 40(10), 16143–16150.

11) Valenzuela, R. (1994). Magnetic Ceramics. Cambridge University Press.

12) Pullar, R. C. (2012). Hexagonal ferrites: A review of the synthesis, properties and applications of hexaferrite ceramics. Progress in Materials Science, 57(7), 1191–1334.

13) Ghasemi, A., et al. (2007). Sol–gel synthesis and characterization of $NiFe_2O_4$ nanoparticles. Journal of Alloys and Compounds, 454(1-2), 420–424.

14) Patange, S. M., et al. (2011). Structural and magnetic properties of sol–gel prepared Mg substituted nickel ferrite nanoparticles. Journal of Magnetism and Magnetic Materials, 323(3-4), 329–334.

15) Reddy, B. P. N., et al. (2009). Synthesis and characterization of Ni-Mg ferrite nanoparticles by auto combustion method. Journal of Alloys and Compounds, 481(1-2), 748–752.

16) Ranjith, R., et al. (2021). Influence of synthesis route on the microstructure and dielectric properties of Mg-doped nickel ferrite nanoparticles. Journal of Materials Science: Materials in Electronics, 32(4), 4212–4222.

17) Nimbalkar, A. V., et al. (2017). Structural, morphological and gas sensing properties of sol–gel synthesized $NiFe_2O_4$ nanoparticles. Sensors and Actuators B: Chemical, 248, 980–988.

18) Singh, A. K., et al. (2016). Structural, electrical and magnetic properties of Mg substituted $NiFe_2O_4$ nanoparticles synthesized via sol–gel method. Journal of Magnetism and Magnetic Materials, 417, 119–124.

19) Shirsath, S. E., et al. (2014). Sol–gel auto-combustion synthesis of Mg substituted $NiFe_2O_4$ nanoparticles: Structural, magnetic and Mössbauer studies. Journal of Alloys and Compounds, 581, 440–446.

20) Nadeem, K., et al. (2018). Structural, dielectric and magnetic properties of $Ni_{1-x}Mg_xFe_2O_4$ ferrite nanoparticles synthesized by sol-gel auto combustion method. Journal of Alloys and Compounds, 763, 1030–10

Effect of waste tea powder infused bio formulation on the germination of seeds

Dr. Savita D. Mali[a], Dr. Komal K. Bhise[a], Dr. Tekchand C. Gaupale[b], Suhasi R. Kamble[a], Vishal M. Patil[a], Sujay P. Parase[a]

[a]Department of Microbiology, Vivekanand College, Kolhapur
(An Empowered Autonomous Institute), Maharashtra, India
[b]Department of Zoology, Vivekanand College, Kolhapur
(An Empowered Autonomous Institute), Maharashtra, India

Abstract

Tea leaves after its utilization for the preparation of non-alcoholic beverage are thrown as it is in the environment. However, leftover tea leaves are good source of plant nutrients. Thus, waste tea leaves powder added with plant beneficial microbes could be useful for plant growth and development. In the present study, seeds treated with a potent phosphate solubilising strain combined with waste tea powder showed earlier germination of seeds and increased root and shoot length over untreated seeds. Thus, the application of tea powder with beneficial bacteria to seeds is an ecofriendly approach for plant development and hence for sustainable agriculture.

Keywords: Food waste, Microbial stimulant, Seed development, Organic fertilizer

1.0 Introduction

Seed germination is an important step in the life cycle of plants. Seeds that germinate quickly have good competence, increased plant growth, and thus increased crop yield over slower-germinating seeds. Several chemical substances are available in the market that can enhance seed germination. However, these chemicals are hazardous to ecosystem (Pan M. et al., 2022). The increasing demand for sustainable and ecofriendly agricultural practices has led to the exploration of novel bioformulations that can enhance seed germination and plant growth. Food waste is a major component of organic waste that has widespread issue in the food system. Globally each year approximately one third of the food produced for human consumption is lost or wasted which constitutes approximately 1.3 billion metric tons. Tea powder is also one component of food waste of organic origin. Tea which is prepared from *Camellia sinesis* leaves is one of the world's most popular non-alcoholic beverages (Tarashkar M. et al., 2023). Tea leaves powder contains nitrogen along with phosphorus and potassium as well as other micro nutrients that are beneficial for soil as well as plants (Mandal S. et al., 2024). These are high in tannic acid which helps to increase oxygenation and facilitates the growth of root system. Similarly, tea powder decomposes easily in landfills and do not cause harm to environment. Tea leaves are effective for fruit bearing plants, herbs, and flowering plants (Lazcano C. and Dońınguez J., 2011). The immense consumption of tea generates thousands of kilos of waste tea powder, most of which is tossed in dustbins, but this waste can actually be used as nutrient rich fertilizer (Debnath B. et al., 2021).

Hence, the application of waste tea in soil is an environment friendly approach over the application of chemicals. Moreover, application of waste tea powder in combination with plant beneficial microbes could be more advantageous for plant development. Soil contains an enormous number and variety of microbial flora which are beneficial for effective seed germination (Garg F., 2024). In context of this, a research study was designed to isolate and wrap a potent plant beneficial bacterial strain in waste tea powder and to study its effect on the germination of seeds.

2.0 Materials and Methods

2.1 Collection of samples

Soil samples were collected from banana field of Sangli district and sugarcane field of Kolhapur district. The soil samples were collected in sterile polythene bags and immediately brought to the laboratory.

Tea powder leftover after preparation of tea was collected in polythene bags and brought to the laboratory. The powder was washed repeatedly with water to remove residual sugar. The powder was dried under sun.

2.2 Isolation of bacteria from soil sample

Serial dilutions of soil samples were done from 10^{-1} to 10^{-6} in the sterile distilled water. 0.1 ml of each dilution was spread on the sterile nutrient agar plates. The plates were labelled properly. These plates were then incubated at room temperature for 24 hrs. After incubation, well isolated bacterial isolates were checked for purity of culture by Gram staining procedure. Pure cultures were labelled as Isolate 1, Isolate 2, and so on. Finally, all pure cultures were stored on nutrient agar slants in refrigerator.

2.3 Screening of bacteria (PSB) on the basis of phosphate solubilization

All pure cultures were spot inoculated on sterile Pikovskaya's agar medium (Pikovskaya R., 1948). Plates were incubated at room temperature for 72 hrs. After incubation plates were examined for development of clear zone around colonies which is the indication of phosphate solubilisation (Babu S. et al., 2017). The bacterial isolates showing phosphate solubilization were further examined for detection of potent phosphate solubilizer (PSB) by calculating solubilization index (Paul D. & Sinha S., 2017).

2.4 Identification of potent PSB isolate

The potent PSB isolate was identified by studying colony characteristics, morphological characteristics (Gram nature, motility, capsule and spore development), and biochemical characteristics (sugar fermentations and other characteristics).

2.5 Study of auxiliary plant beneficial characteristics of potent PSB isolate

2.5.1 Study of nitrogen fixation ability

The potent Isolate 6 was inoculated on nitrogen-free bromothymol blue (NFB) agar medium. The colour change of the medium from green to blue around growth confirms nitrogen fixation by bacteria (Nakbanpote W. et al., 2014).

2.5.2 Study of ammonia production

A loopful suspension of potent isolate was inoculated in peptone water broth. After incubation, 0.5 ml Nessler's reagent was added and ammonia production was identified on the basis of development of brown to yellow colour in the tube (Bhattacharyya C. et al., 2020).

2.5.3 Study of salt tolerance ability

A fresh suspension of the potent isolate no. 6 was inoculated in nutrient broth containing various concentrations of NaCl (1 to 10%) and KCl (1 to 10%) separately. All tubes were examined for turbidity after incubation at RT for 24 hrs (Sharma A. et al., 2021).

2.6 Antibiotic sensitivity testing

The potent isolate was examined for sensitivity towards different antibiotics like amoxicillin (AMx10), penicillin-G (P10), ofloxacin (OF5), ciprofloxacin (C15), chloramphenicol (C30), and tetracycline (TE30) by agar well diffusion method (Taoufiq K. et al., 2024).

2.7 Preparation of tea powder-based bio formulation

Dry leftover tea powder was sterilised by autoclaving. It was then added with 24 hr old nutrient broth culture of potent isolate 6. This bio formulation was incubated at RT for 24 hrs.

2.8 Seed germination studies

Seeds of *Vigna radiata* (Mung bean) were surface sterilised and subsequently washed repeatedly with sterile distilled water. Various treatments were given to seeds.

Treatment 1: Untreated seeds (control)

Treatment 2: Seeds were treated with Isolate 6 alone

Treatment 3: Seeds were treated with waste tea powder alone

Treatment 4: Seeds were treated with novel bio formulation containing waste tea powder and Isolate 6

All seeds were then placed on moist cotton bed in separate sterile Petri plates. Plates were labelled properly. Everyday germination of seeds of each treatment was examined.

3.0 Results and Discussion

3.1 Isolation of bacteria and screening of PSB

Table 1 Screening of bacterial isolates on the basis of phosphate solubilization

Isolate name	Phosphate solubilisation
Isolate 1	+
Isolate 2	+
Isolate 3	-
Isolate 4	+
Isolate 5	-
Isolate 6	+
Isolate 7	+
Isolate 8	+
Isolate 9	+
Isolate 10	-

Isolate 11	-
Isolate 12	-

+ Phosphate solubilisation; - No phosphate solubilization

More than 50 bacterial isolates were obtained from soil samples on nutrient agar media. Based on the morphological studies, 12 purified isolates with diverse morphology when studied for phosphate solubilisation, 7 isolates coded as Isolate 1, Isolate 2, Isolate 4, Isolate 6, Isolate 7, Isolate 8, and Isolate 9 showed phosphate solubilisation, while 5 isolates labelled as Isolate 3, Isolate 5, Isolate 10, Isolate 11, and Isolate 12 seen failed to solubilise phosphate (Table 1). The assessment of phosphate solubilization of all positive isolates revealed Isolate 6 as most effective phosphate solubilizer on the basis of solubilization index (Table 2)

Table 2 Screening of most potent phosphate solubilizer

Isolate code	Colony diameter (cm) (A)	Zone diameter (cm) (B)	Solubilization index SI = B/A
Isolate 1	0.5	1.2	2.40
Isolate 2	0.4	0.6	1.50
Isolate 3	0.4	No zone	-
Isolate 4	0.5	1.0	2.0
Isolate 5	0.3	No zone	-
Isolate 6	0.5	1.3	**2.60**
Isolate 7	0.5	0.7	1.40
Isolate 8	0.3	0.5	1.66
Isolate 9	0.5	0.6	1.20
Isolate 10	0.4	No zone	-
Isolate 11	0.2	No zone	-
Isolate 12	0.2	No zone	-

3.2 Identification of potent PSB isolate

Identification characteristics of Isolate 6 are represented in Table 3

Table 3 Identification of potent Isolate 6

Colony characteristics	
Size	Diameter = 1mm
Shape	Circular
Colour	White
Opacity	Opaque
Margin	Entire
Elevation	Convex
Surface	Smooth
Consistency	Sticky
Morphological characteristics	
Gram nature	Gram positive cocci arranged in clusters
Motility	Non motile

Spore formation	Non spore former
Capsule formation	No capsule
Biochemical characters	
Glucose	+
Lactose	-
Maltose	-
Sucrose	-
Ribose	+
Galactose	-
Mannitol	-
Catalase	+
Urease	-
Gelatinase	+

+ Utilization of sugar/Production of enzyme;

- No utilization of sugar/No production of enzyme

3.3 Study of auxiliary plant beneficial characteristics of potent PSB Isolate 6

Table 4 Plant beneficial characteristics of potent PSB Isolate 6

Characteristic	Result
Nitrogen fixation	+
Ammonia production	+
Amylase activity	+
NaCl tolerance	Turbidity up to 7% NaCl
KCl tolerance	Turbidity up to 8% KCl

The isolate showed growth on nitrogen-free bromothymol blue (NFB) agar medium with colour change of the medium from green to blue around growth indicating fixation of nitrogen. Similarly, change in the colour of peptone water broth culture after addition of Nessler's reagent confirmed ammonia production by isolate. The isolate also observed to have amylase activity (Table 4). Salt tolerance studies revealed that the isolate tolerate high percentage of salt (Table 4) indicating that the isolate can also be applied in saline soils.

3.4 Antibiotic sensitivity testing

The potent Isolate 6 when analysed for its sensitivity towards various antibiotics, it was observed that the isolate is sensitive to chloramphenicol, ciprofloxacin, tetracycline, and ofloxacin and resistant to penicillin-G and amoxicillin (Table 5). The sensitivity of isolate towards number of antibiotics suggests that the usage of isolate is safe for environment.

Table 5 Sensitivity of Isolate 6 to various antibiotics

Name of antibiotic	Short form	Inhibition zone (mm)
Chloramphenicol	C30	1.5

Ciprofloxacin	C15	2
Tetracycline	TE30	1
Penicillin-G	P10	-
Amoxicillin	AMX10	-
Ofloxacin	OF5	2

- No inhibition zone

3.5 Study of seed germination

Table 6 Effect of tea powder based bio formulation on germination of *Vigna radiata*

Parameters/ Treatments	% of germination (after 24 hrs.)	Radical length in cm (average of 10 seeds) After 5 days	Shoot length in cm (average of 10 seeds) After 5 days
Untreated seeds (Control)	0	0.51	1.72
Seeds treated with Isolate 6 only	53	1.84	4.32
Seeds treated with waste tea powder only	49	1.56	4.02
Seeds treated with bio formulation of tea powder and Isolate 6	60	2.68	6.66

The studies on seed germination indicated that seeds coated with waste tea powder based bio formulation of Isolate 6 have earlier germination than untreated seeds. Simultaneously, seed germination was more in case of seeds treated with bio formulation as compared to seeds treated with Isolate 6 only as well as seeds treated with waste tea powder only. Similarly, assessment of shoot length showed nearly 4 times increase in the average shoot length of bio formulation treated seeds over untreated seeds. The study of radical length of seeds indicated that bio formulated seeds are having nearly 2 fold increase over untreated seeds. The seeds germination research demonstrated that seeds treated with waste tea powder alone and Isolate 6 alone are benefited more as compared to untreated seeds. However, tea powder in combination with Isolate 6 seen more advantageous for seed germination than when applied alone (Table 6). The positive effect of earlier germination, and increased shoot and root length in bio formulated treated seeds may be contributed by nutrients present in waste tea powder as well as because of supply of various nutrients by Isolate 6.

4.0 Conclusion

The study demonstrates the potential of waste tea powder infused bioformulation as a sustainable and eco-friendly approach to enhance seed germination and promote plant growth. The findings suggest that waste tea powder can provide essential nutrients and bioactive compounds that improve seed germination rates and hence plant productivity. The usage of waste tea powder can also help to reduce waste disposal issues. Moreover, usage of bacterial culture with waste tea powder further improves seed germination. Thus,

bio formulations based on waste tea powder may offer a cost – effective alternative to synthetic fertilizers and growth promoters for plants.

5.0 References

1. Babu, S. V., Triveni, S., Reddy, R. S., & Sathyanarayana, J. (2017). Screening of maize rhizosperic phosphate solubilizing isolates for plant growth promoting characteristics. *Int J Curr Microbiol App Sci*, *6*(10), 2090-2101.

2. Bhattacharyya, C., Banerjee, S., Acharya, U., Mitra, A., Mallick, I., Haldar, A., ... & Ghosh, A. (2020). Evaluation of plant growth promotion properties and induction of antioxidative defense mechanism by tea rhizobacteria of Darjeeling, India. *Scientific reports*, *10*(1), 15536.

3. Debnath, B., Haldar, D., & Purkait, M. K. (2021). Potential and sustainable utilization of tea waste: A review on present status and future trends. *Journal of Environmental Chemical Engineering*, *9*(5), 106179.

4. Garg, F. C. (2024). Role of Microorganisms in Seed Germination.In *New Perspectives on Seed Germination*. IntechOpen.

5. Lazcano, C., & Domínguez, J. (2011). The use of vermicompost in sustainable agriculture: impact on plant growth and soil fertility. *Soil nutrients*, *10*(1-23), 187.

6. Mandal, S., Yadav, A., Kumar, S., &Mura singh, S. (2024). An extensive review study on bioresources recovery from tea waste and its emerging applications. *Waste Management Bulletin*, *2*(4), 155-166.

7. Nakbanpote, W., Panitlurtumpai, N., Sangdee, A., Sakulpone, N., Sirisom, P., & Pimthong, A. (2014). Salt-tolerant and plant growth-promoting bacteria isolated from Zn/Cd contaminated soil: identification and effect on rice under saline conditions. *Journal of Plant Interactions*, *9*(1), 379-387.

8. Pan, M., Yau, P. C., Lee, K. C., & Man, H. Y. (2022). Effects of different fertilizers on the germination of tomato and cucumber seeds. *Water, Air, & Soil Pollution*, *233*(1), 25.

9. Paul, D., & Sinha, S. N. (2017). Isolation and characterization of phosphate solubilizing bacterium Pseudomonas aeruginosa KUPSB12 with antibacterial potential from river Ganga, India. *Annals of Agrarian Science*, *15*(1), 130-136.

10. Pikovskaya, R. I. (1948). Phosphate mobilization in soils as related to life processes of some microorganisms. *Mikrobiologiya*, *17*, 362-370.

11. Sharma, A., Dev, K., Sourirajan, A., & Choudhary, M. (2021). Isolation and characterization of salt-tolerant bacteria with plant growth-promoting activities from saline agricultural fields of Haryana, India. *Journal of Genetic Engineering and Biotechnology*, *19*(1), 99.

12. Taoufiq, K., Aberchane, L., Amri, O., Oufdou, K., El Biari, K., Talbi, A., ... &Faghire, M. (2024). Antibiotics resistance and PGPR traits of endophytic bacteria isolated in arid region of Morocco. *International Journal of Plant Biology*, *15*(4), 1063-1076.

13. Tarashkar, M., Matloobi, M., Qureshi, S., & Rahimi, A. (2023). Assessing the growth-stimulating effect of tea waste compost in urban agriculture while identifying the benefits of household waste carbon dioxide. *Ecological Indicators*, *151*, 110292.

Effect of poultry waste derived feather degraded lysate on seed germination and growth of *V radiata* L.

Dr. Komal K. Bhise[1*], Dr. Savita D. Mali[1], Dr Tekchand C. Gaupale[2], Indrayani R. Bhandigare[1], Naziya R. Desai[1], Aditya D. Patil[1]

Department of Microbiology, Vivekanand College, Kolhapur (An Empowered Autonomous Institute), Maharashtra, INDIA

Department of Zoology, Vivekanand College, Kolhapur (An Empowered Autonomous Institute), Maharashtra, INDIA

Abstract:

The accumulation of feather waste from poultry operations represents an environmental challenge due to its high keratin content and resistance to natural breakdown. In the present study, microorganisms were isolated from soil collected at a poultry dumping site. Among the isolates obtained, KM1, KM7, and KM11 demonstrated feather-degrading capabilities, with KM11 showing the most pronounced activity. The feather lysate produced by KM11 was evaluated for its effects on the growth of *Vigna radiata* L. (mung bean). Seeds treated with the KM11 lysate exhibited improved germination compared to untreated controls. Plant growth analysis was done after 7 and 14 days revealed significant increases in shoot and root length, fresh and dry weight and chlorophyll content, indicating the potential of feather degraded lysate to act as a natural plant growth promoter. These results suggest that KM11 could serve a dual role in biodegrading poultry waste and promoting sustainable plant growth.

Keywords: Feather waste, Feather lysate, *Vigna radiata*, Plant Growth

Introduction-:

Nowadays, with the growth of the poultry industry, huge quantities of waste are produced reaching millions of tons annually (Da Silva et al. 2018; Verma et al. 2018). This creates complex challenges, particularly in managing the large volumes of waste it generates among these, chicken feathers constitute a significant portion. This waste poses serious environmental challenges, contributes to climate-related issues and may adversely affect human health. (Williams et al. 1990). Common disposal methods such as landfilling and incineration, not only contribute to environmental pollution but also result in the loss of valuable components like proteins and enzymes (Lasekan et al. 2013).

Chicken feathers are an abundant and low-cost source of protein, with significant potential for use as bio-fertilizers. Through microbial degradation, feathers can be broken down into a lysate rich in amino acids and peptides. This lysate acts as a biostimulant, enhancing nutrient absorption, promoting plant growth and improving resistance to both abiotic and biotic stresses, ultimately contributing to increased crop yields (Bhise et al. 2017)

Sustaining high agricultural productivity is essential to meet the food demands of the growing global population. To achieve this, synthetic fertilizers are widely used; however, their excessive application often leads to runoff into water bodies, resulting in eutrophication and environmental degradation. To mitigate the environmental risks associated with the excessive use of chemical fertilizers, organic fertilizers and biofertilizers have gained recognition as key components of sustainable agricultural practices (Abdel-Hamid et al. 2021). Among these, the development of bio-fertilizers from chicken feather waste is drawing significant attention from researchers, agronomists and environmentalists due to its potential as a sustainable and eco-friendly solution (Tiwari and Gupta 2010). Feather meal, containing approximately 15% nitrogen, is

an inexpensive and readily available nitrogen source, making it a promising candidate for use as a bio-fertilizer. Additionally, protein hydrolysate derived from feathers have shown potential in promoting plant growth, further supporting their application in agriculture. Therefore, microbial degradation of feathers offers a sustainable approach for producing slow-release fertilizers that enhance soil fertility and support long-term crop productivity (Hadas and Kautsky 1994).

In present study, we have isolated feather degrading organism from poultry dumped soil. The isolates were tested for proteolytic activity and feather degradation ability. The feather degradation was studied by evaluating released proteins and amino acids content. The effect of feather degraded lysate of KM11 on seed germination and growth of *Vigna radiata* L. was studied and plant analysis was done after 7 and 14 days of growth.

Material and methods

Collection of soil sample

The soil sample is collected from poultry feathers dumping site from Sangli and Kolhapur district nearby areas. The six representative soil samples were collected in sterile polythene bags and transported to the laboratory.

Isolation of organisms from the soil sample

One gram of soil sample was taken and it was serially diluted from 10^{-1} to 10^{-10}. 0.1 ml of soil dilution was spread on sterile Skim milk agar plates for detecting the proteolytic activity. The plates were incubated at 37°C for 24-48 hrs morphologically distinct bacterial colonies were selected and purified cultures were preserved for further study.

Feather degradation study

One loopful of bacterial culture was inoculated into the poultry feather minimal media containing chicken feathers (PFM) as sole source of carbon and nitrogen and was kept under shaking condition (150 rpm) at RT for 4-5 days. After every 24 hrs feather degradation was studied by evaluating proteins and amino acids contents of CFM (Bhise et al. 2017).

Protein Estimation

Protein estimation was performed by using Lowry method ((Lowry et al. 1951). Briefly, 0.5 ml of sample was mixed with 2.5 ml of freshly prepared alkaline copper reagent (a mixture of 2% Na_2CO_3 in 0.1 N NaOH, 0.5% $CuSO_4 \cdot 5H_2O$ and 1% sodium potassium tartrate). After a 10-minute incubation at room temperature, 0.25 ml of diluted Folin–Ciocalteu reagent was added and the mixture was incubated in the dark for 30 minutes. Absorbance was measured at 750 nm. The concentration of protein was determined using BSA (bovine serum albumin) as standard.

Amino acid Estimation

Amino acids was estimated using method of Moore and Stein (1954). Briefly, 1.0 ml of the sample was combined with 1.0 ml of 0.1% ninhydrin reagent prepared in citrate buffer (pH 5.5). The reaction mixture was incubated in a boiling water bath for 15 minutes to facilitate the formation of the Ruhemann's purple chromophore. Following incubation, tubes were cooled to room temperature and absorbance was recorded at 570 nm using a UV-Visible spectrophotometer. Quantification was performed by comparison with a standard leucine curve.

Characterization and identification of potent isolate

Morphological and biochemical characteristics of potent organism was studied to identify genus of organism.

In vitro plant growth studies

Seed germination study

The seeds of *Vigna radiata* were surface sterilized with 70% ethanol for 10 mins and washed several times with distilled water. Surface sterilized seeds were treated with feather degraded lysate (FL) and control set (CS) was treated with water and germination was studied after 7 days (Abdel-Aziz et al 2014).

$$\text{Germination \%} \quad \frac{\text{Number of germinated seeds}}{\text{Number of total seeds}} \quad \text{X } 100$$

Pot study

The effect of feather degraded lysate to promote growth of plant was tested by pot trials. Pot study was carried out in September with average humidity of 30% and temperature 32-35° C. Soil was autoclaved for sterilization. Seeds used for experiment was surface sterilized using ethanol (70%) and washed repeatedly with sterile distilled water. The surface sterilized seeds were sown into pot and FL set was inoculated separately with feather degraded lysate (5ml) of KM1, KM7 and KM11 and CS with water only. After 7 and 14 days of growth seedlings was uprooted and plant analysis was performed to evaluate effect of feather degraded lysate on growth of plant (Bhise et al. 2017).

Plant analysis

The shoot and root length, fresh plus dry weight of FL and control set seedlings were measured and noted down. The chlorophyll content of control and feather degraded lysate was estimated using method of Arnon (1949).

Statistical analysis

All the experiments were run in triplicates and data values were expressed as mean±S.D. One way ANOVA was applied using Minitab (release 19) on data to find efficacy.

Result and Discussion

Isolation of organisms from soil

Fifty-nine organisms were isolated from different soil samples. Out of these, thirteen organisms showed maximum proteolysis zone on skim milk agar plates. These thirteen organisms were used for further study.

Feather degradation study

Ability of thirteen potent organisms to degrade poultry feathers were tested using PFM. Among thirteen organisms, three organisms (KM1, KM7 and KM11) showed highest feather degradation after 72 hrs of incubation. The released proteins and amino acids were evaluate after every 24 hrs. The amount of

proteins released during feather degradation was highest after 72 hrs and reduced after 96 hrs (Fig.1). Similarly, amino acid contents was also analyzed and it was maximum after 96 hrs and declined after 120 hrs (Fig. 2). Among three isolates, KM11 was highly potent in feather degradation ability (Fig.1 and 2).

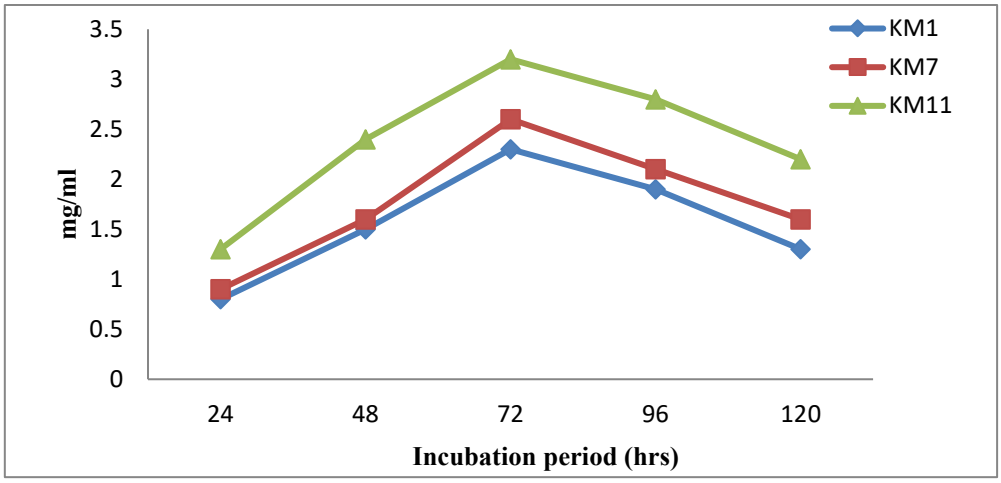

Fig 1. Estimation of protein content of feather degraded lysate

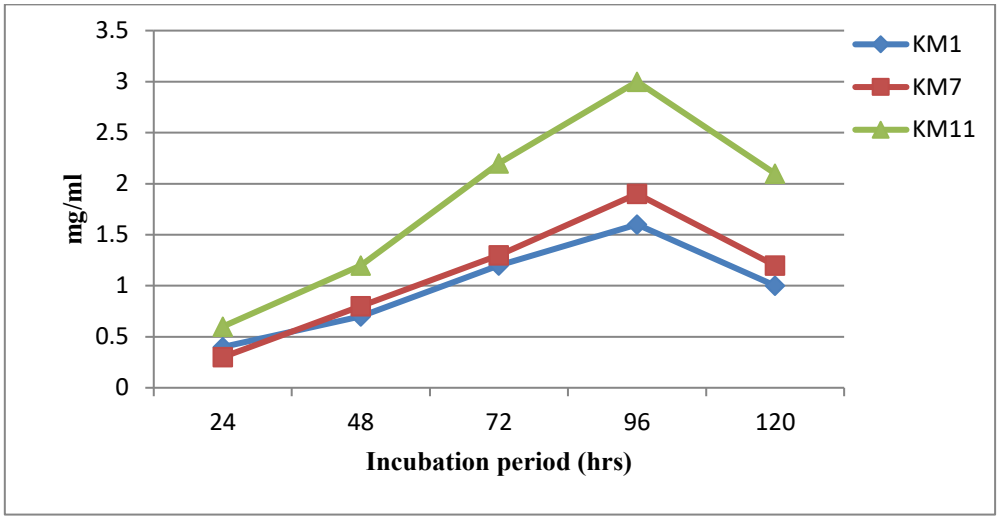

Fig 2. Estimation of amino acid content of feather degraded lysate

Characterization and identification of potent isolate

The KM11 was gram positive rod shaped motile organism. The isolate showed glucose, fructose, sucrose, maltose, mannitol, mannose and xylose sugar fermentation. It also showed catalase and gelatin hydrolysis. IMVic test was also performed and organism showed negative indole plus methyl red test while voges proskauer and citrate utilization test were positive. These results indicates that the KM11 isolate belongs to *Bacillus subtilis* genera however 16S rDNA sequence analysis is required to confirm identity of organism.

Seed germination

Feather degraded lysate inoculated seeds showed highest germination compared to control set. Germination study clearly indicated the potency of KM1, KM7 and KM11 in germinating seeds of *V. radiate.* Among these three lysates, KM11 was found to be potent in supporting seed germination after 7 days of growth (Fig.3). similarly, Paul et al. (2013) also reported improved growth and germination (87.5%) of *Cicer arietinum* supplied with feather lysate.

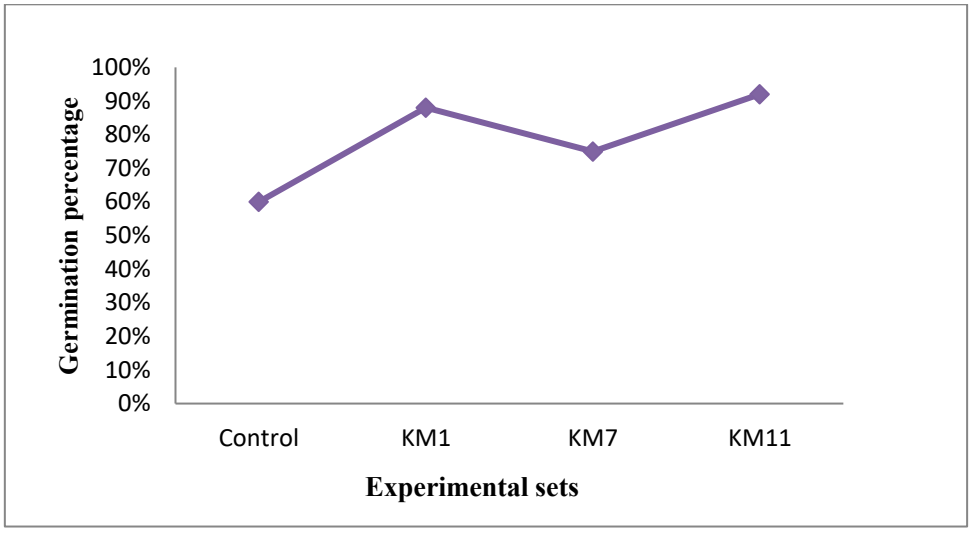

Fig 3. Effect of FL on seed germination

Plant analysis

Researchers have successfully identified various microorganisms from different habitats that possess the ability to degrade keratin, enabling the transformation of keratin-rich waste materials into commercially valuable products (de Menezes et al. 2021). The isolated microorganisms demonstrated the capability to break down keratin and keratin-rich wastes such as feathers into soluble compounds and amino acids (Callegaro et al. 2018; Bohacz, 2019; Chaudhary et al. 2021) that can supports the growth of plant.

Effect of FL on growth of plant was studied and analysis was done after 7 and 14 days. FL inoculated plants showed significantly improved root and shoot length compared to control plants (Fig. 4).

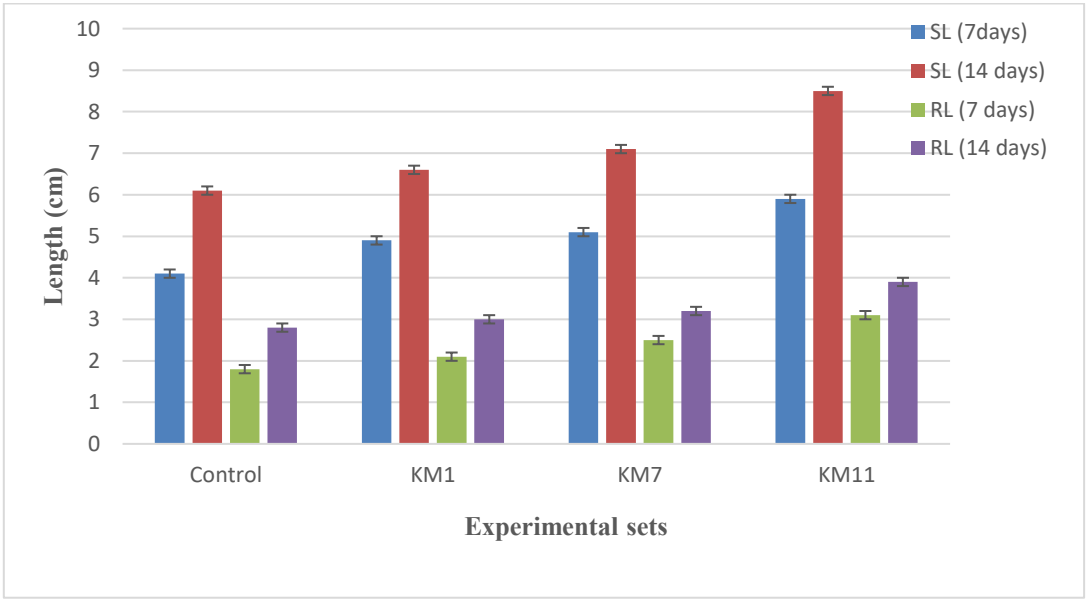

Fig 4. Effect of FL on plant length

KM1, KM7 and KM11 was effective in promoting shoot and root length after 7 and 14 days. KM11 was found to be highly effective in promoting both root and shoot length followed by KM 7 and KM1 (Fig.4). Similarly, the complete degradation of chicken feathers yielded a feather hydrolysate that significantly promoted the growth of *Vigna radiata* var. *meha* (mung bean) (Bose et al. 2014). The Peptides

present in keratin hydrolysate may exhibit hormone-like activity contributing to plant growth regulation. Additionally, these compounds can indirectly enhance nutrient uptake and utilization thereby supporting overall plant growth development (Raguraj et al. 2022).

Effect of lysate on fresh weight of plant was also studied. KM 11 improved fresh weight of seedlings by 64 % after 7 days and 57 % after 14 days of growth (Fig.5). Similarly, dry weight of seedling was increased 90 % and 70 % when supplemented with KM11 after 7 and 14 days of growth respectively (Fig. 5). The amino acids present in keratin hydrolysate can serve as a nitrogen source for rhizospheric microorganisms, influencing their activity in the root zone and thereby affecting plant growth and development. KM11 exhibited highest ability to degrade feathers hence plants inoculated with FL showed improved length and weight.

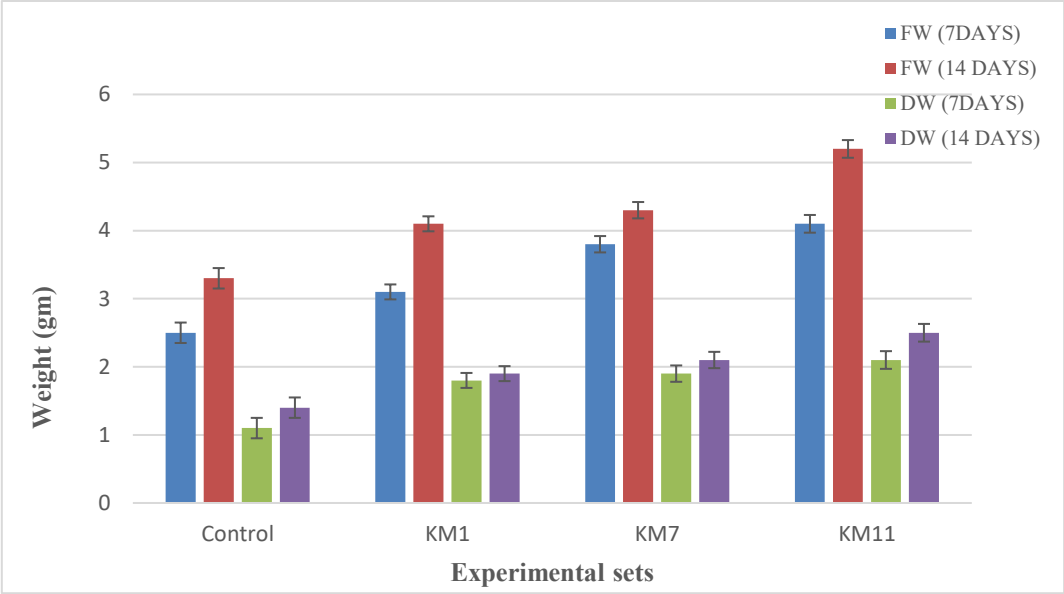

Fig 5. Effect of FL on plant weight

Studies have demonstrated that microbial keratin hydrolysate can effectively promote plant growth, making it a sustainable alternative to conventional fertilizers (Moe, 2013). Nafady et al. (2018) reported a strain of *Bacillus licheniformis* ASU with the ability to degrade chicken feathers, In addition, this strain demonstrated phosphate-solubilizing activity and produced high levels of indole-3-acetic acid (IAA). Presence of lysate along with such plant growth promoting traits accelerates plant growth.

Plants inoculated with FL also showed improved chlorophyll content as compared to control. Out of three lysates studied, KM11 was more impactful in improving photosynthesis activity compared to KM1 and KM7. KM11 improved chlorophyll content by 60 and 43 % after 7 and 14 days respectively. KM1 and KM7 improved chlorophyll content by 29 and 39 % after 7 days and 10 and 23% after 14 days of growth (Fig.6).

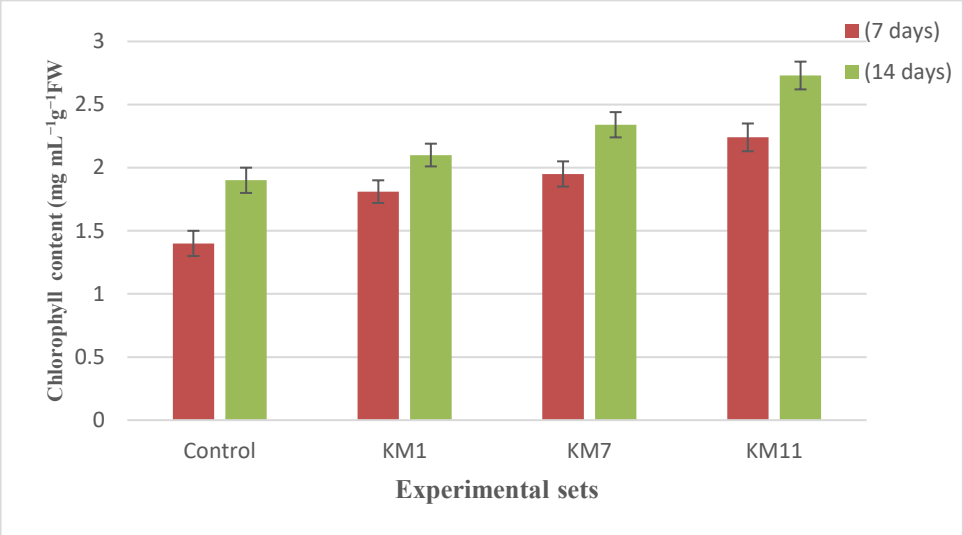

Fig 6. Effect of FL on plant chlorophyll content

Microbial keratin hydrolysate applied to soil enhance the soil microbiome by stimulating the proliferation of beneficial microorganisms involved in biological nitrogen fixation, as well as in the solubilization and mobilization of phosphate and potassium ions. Availability of such nutrients along with beneficial organism improves chlorophyll content of plants. Due to its composition of viable microbial populations combined with essential macro- and micronutrients, microbial keratin hydrolysate qualifies as a biofertilizer, contributing to improved nutrient cycling and soil fertility (Kumar et al. 2022).

Conclusion

The present study demonstrates the promising potential of feather-degraded lysate inoculum, KM11 in enhancing seed germination, plant growth and soil fertility. The enzymatic breakdown of keratin-rich feathers by microbial action not only provides a sustainable method for managing poultry waste but also generates nutrient-rich byproducts beneficial to plant development. Application of this lysate, especially when combined with beneficial microorganisms, led to improved seed germination, length, weight and chlorophyll content in *Vigna radiata* L. Moreover, the incorporation of feather hydrolysate into soil contributes to its nutrient profile, particularly by supplying nitrogen and amino acids, which are vital for plant metabolism. These findings suggest that microbial feather degradation can be effectively integrated into agricultural practices as a biofertilizer strategy, potentially leading to higher crop yields and reduced dependency on synthetic fertilizers. Continued research and field-scale validation may further establish its role in sustainable and eco-friendly farming systems

Conflict of interest

The authors declare that they have no conflict of interest

References

- Abdel-Aziz, S. M., Moustafa, Y. A., & Hamed, H. A. (2014). Lactic acid bacteria in the green biocontrol against some phytopathogenic fungi: treatment of tomato seeds. *Journal of Basic and Applied Scientific Research*, *4*(12), 1-9.
- Abdel-Hamid, M. S., Fouda, A., El-Ela, H. K. A., El-Ghamry, A. A., and Hassan, S. E.-D. (2021). Plant growth-promoting properties of bacterial endophytes isolated from roots of Thymus vulgaris L. and investigate their role as biofertilizers to enhance the essential oil contents. Biomol. Concepts. 12, 175–196. doi: 10.1515/bmc-2021-0019

- Arnon, D. I. (1949). Copper enzymes in isolated chloroplasts. Polyphenoloxidase in Beta vulgaris. *Plant physiology*, *24*(1), 1.
- Bhise, K. K., Bhagwat, P. K., & Dandge, P. B. (2017). Synergistic effect of Chryseobacterium gleum sp. SUK with ACC deaminase activity in alleviation of salt stress and plant growth promotion in Triticum aestivum L. *3 Biotech*, *7*(2), 105.
- Bohacz, J. (2019). Changes in mineral forms of nitrogen and sulfur and enzymatic activities during composting of lignocellulosic waste and chicken feathers. Environ. Sci. Pollut. Res. 26, 10333–42. doi: 10.1007/s11356-019-04453-2
- Bose, A., Pathan, S., Pathak, K., & Keharia, H. (2014). Keratinolytic protease production by Bacillus amyloliquefaciens 6B using feather meal as substrate and application of feather hydrolysate as organic nitrogen input for agricultural soil. *Waste and biomass valorization*, *5*(4), 595-605.
- Callegaro, K., Welter, N., and Daroit, D. J. (2018). Feathers as bioresource: microbial conversion into bioactive protein hydrolysates. Proc. Biochem. 75, 1–9. doi: 10.1016/j.procbio.2018.09.002
- Chaudhary, L., Siddiqui, M. H., Vimal, A., and Bhargava, P. (2021). Biological degradation of keratin by microbial keratinase for effective waste management and potent industrial applications. Curr. Protein Pept. Sci. doi: 10.2174/1389203722666210215151952
- Da Silva, R. R. (2018). Keratinases as an alternative method designed to solve keratin disposal on the environment: its relevance on agricultural and environmental chemistry.
- de Menezes, C. L. A., Santos, R. D. C., Santos, M. V., Boscolo, M., da Silva, R., Gomes, E., et al. (2021). Industrial sustainability of microbial keratinases: production and potential applications. World J. Microbiol. Biotechnol. 37, 86. doi: 10.1007/s11274-021-03052-z
- Hadas, A., & Kautsky, L. (1994). Feather meal, a semi-slow-release nitrogen fertilizer for organic farming. *Fertilizer research*, *38*(2), 165-170.
- Kumar, S., Diksha, S. S. S., and Kumar, R. (2022b). Biofertilizers: An ecofriendly technology for nutrient recycling and environmental sustainability. CRMICR. 3, 100094. doi: 10.1016/j.crmicr.2021.100094
- Lasekan, A., Bakar, F. A., & Hashim, D. (2013). Potential of chicken by-products as sources of useful biological resources. *Waste management*, *33*(3), 552-565.
- Lowry, O. H., Rosebrough, N. J., Farr, A. L., & Randall, R. J. (1951). Protein measurement with the Folin phenol reagent. *J biol Chem*, *193*(1), 265-275.
- Moe, L. A. (2013). Amino acids in the rhizosphere: From plants to microbes. Am. J. Bot. 100, 1692–1705. doi: 10.3732/ajb.1300033
- Moore, S., & Stein, W. H. (1954). A modified ninhydrin reagent for the photometric determination of amino acids and related compounds.
- Nafady, N. A., Hassan, E. A., Abd-Alla, M. H., & Bagy, M. M. K. (2018). Effectiveness of eco-friendly arbuscular mycorrhizal fungi biofertilizer and bacterial feather hydrolysate in promoting growth of Vicia faba in sandy soil. *Biocatalysis and agricultural biotechnology*, *16*, 140-147.
- Paul, T., Halder, S. K., Das, A., Bera, S., Maity, C., Mandal, A., ... & Mondal, K. C. (2013). Exploitation of chicken feather waste as a plant growth promoting agent using keratinase producing novel isolate Paenibacillus woosongensis TKB2. *Biocatalysis and Agricultural Biotechnology*, *2*(1), 50-57.
- Raguraj, S., Kasim, S., Md Jaafar, N., & Nazli, M. H. (2022). Growth of tea nursery plants as influenced by different rates of protein hydrolysate derived from chicken feathers. *Agronomy*, *12*(2), 299.

- Tamreihao, K., Mukherjee, S., Khunjamayum, R., Devi, L. J., Asem, R. S., and Ningthoujam, D. S. (2019). Feather degradation by keratinolytic bacteria and biofertilizing potential for sustainable agricultural production. J. Basic Microbiol. 59, 4–13. doi: 10.1002/jobm.201800434
- Tiwary, E., & Gupta, R. (2010). Medium optimization for a novel 58ákDa dimeric keratinase from Bacillus licheniformis ER-15: Biochemical characterization and application in feather degradation and dehairing of hides. *Bioresource technology*, *101*(15), 6103-6110.
- Verma, A., Singh, H., Anwar, S., Chattopadhyay, A., Tiwari, K. K., Kaur, S., et al. (2017). Microbial keratinases: industrial enzymes with waste management potential. Crit. Rev. Biotechnol. 37, 476–491. doi: 10.1080/07388551.2016.1185388
- Vernieri, P. A. O. L. O., Borghesi, E., Tognoni, F., Serra, G., Ferrante, A., & Piagessi, A. (2006, October). Use of biostimulants for reducing nutrient solution concentration in floating system. In *III International Symposium on Models for Plant Growth, Environmental Control and Farm Management in Protected Cultivation 718* (pp. 477-484).
- Williams, C. M., Richter, C. S., MacKenzie Jr, J. M., & Shih, J. C. (1990). Isolation, identification, and characterization of a feather-degrading bacterium. *Applied and environmental microbiology*, *56*(6), 1509-1515.

Synthesis and Characterization of MnO_2 by Hydrothermal Method for Supercapacitor

Pradip P. Gaikwad[1], Rajaram S. Sutar[2], Akshay R. Jundle[1], Rutuja A. Ekunde[1], Sagar S. Ingole[1], Sanjay S. Latthe[1]*

[1] Self-cleaning Research Laboratory, Department of Physics, Vivekanand College, Kolhapur (An Empowered Autonomous Institute), (Affiliated to Shivaji University, Kolhapur), Kolhapur – 416003, Maharashtra, India.

[2] School of Chemistry and Molecular Sciences, Henan University, Kaifeng, China.

*Corresponding author E-mail: latthes@gmail.com

Abstract

In this study, manganese dioxide (MnO_2) nanowires were successfully synthesized via a hydrothermal method and evaluated for their electrochemical performance as pseudocapacitor materials. The synthesis was carried out under varying temperature conditions (80 °C, 100 °C, and 120 °C), and the resulting structures were characterized using X-ray diffraction (XRD). XRD analysis confirmed a body-centred tetragonal phase with sharp diffraction peaks, indicating high crystallinity and phase purity. Electrochemical characterization, including cyclic voltammetry (CV), galvanostatic charge-discharge (GCD), and electrochemical impedance spectroscopy (EIS), demonstrated excellent capacitive behaviour. The optimized MnO_2 nanowire electrode exhibited a high specific capacitance of 1066 F/g at low scan rates, with good reversibility and minimal internal resistance. GCD curves showed symmetrical charge-discharge profiles, while EIS indicated low charge-transfer resistance and fast ion diffusion.

Keywords: MnO_2 nanowires, hydrothermal synthesis, supercapacitor, specific capacitance, electrochemical performance

1. Introduction

The growing demand for efficient and sustainable energy storage systems has intensified interest in supercapacitors, also known as electrochemical capacitors, due to their superior power density, rapid charge-discharge capabilities, and long cycle life [1]. These characteristics make them particularly attractive for next-generation applications, including electric vehicles, portable electronics, hybrid energy systems, and aerospace technologies [2]. Compared to conventional batteries, supercapacitors bridge the gap between batteries and dielectric capacitors by offering faster dynamics and better durability, although their energy density remains relatively lower [3]. Supercapacitors are typically classified into two major categories based on their charge storage mechanisms: (i) electric double-layer capacitors (EDLCs), which rely on electrostatic charge accumulation at the electrode-electrolyte interface, and (ii) pseudocapacitors, where a charge is stored through fast and reversible faradaic redox reactions [4]. While EDLCs commonly employ carbon-based materials, pseudocapacitive electrodes are often composed of transition metal oxides or conducting polymers, which provide higher specific capacitance due to their redox activity [5].

Among various pseudocapacitive materials, manganese dioxide (MnO_2) has emerged as a particularly promising candidate due to its natural abundance, environmental benignity, low cost, and high theoretical specific capacitance (~1370 F/g [6, 7]. MnO_2 also exhibits multiple polymorphic forms (α-, β-, γ-, δ-, λ-, and ε-), with β-MnO_2 being thermodynamically the most stable. These polymorphs differ in their tunnel structures, which significantly affect ion diffusion and electrochemical performance [8, 9]. Furthermore, MnO_2-based materials possess excellent electrochemical reversibility and high oxidation states, enabling multiple electron-transfer processes during redox reactions [10].

Despite these advantages, bulk MnO_2 suffers from low electrical conductivity (~10^{-5} to 10^{-6} S/cm) and limited active site accessibility, leading to poor rate capability and low practical capacitance [11]. To overcome these challenges, nanostructured MnO_2 has been explored as a strategy to enhance surface area, improve ion transport kinetics, and optimize electron pathways [12]. Synthesis methods such as sol-gel processing, hydrothermal and solvothermal techniques, chemical precipitation, electrochemical deposition, and microwave-assisted methods have

been widely employed to control the morphology and crystallinity of MnO_2 nanostructures [13]. Among these, hydrothermal synthesis has gained particular attention due to its cost-effectiveness, environmental friendliness, and ability to produce one-dimensional architectures such as nanorods and nanowires that are favorable for fast charge transport [14]. In addition to its use in supercapacitors, MnO_2 has also demonstrated potential in other technological applications, including lithium-ion batteries, zinc-ion batteries, fuel cell catalysts, biosensors, and environmental remediation [15]. However, achieving an optimal balance between conductivity, structural stability, and electrochemical performance remains a major research challenge. The electrochemical behavior of MnO_2 is strongly influenced by its morphology, phase composition, and particle size, highlighting the need for precise control over synthesis parameters [16].

In this study, we report the synthesis of [insert synthesis strategy: e.g., hydrothermally derived α-MnO_2 nanorods] and evaluate their electrochemical performance as electrode materials for pseudocapacitor applications. The relationship between morphology, structure, and capacitive behavior is systematically investigated to provide insights into the design of high-performance MnO_2-based energy storage devices.

2. Experimental

2.1 Material

Potassium Permagnate ($KMnO_4$) and hydrochloric acid (HCL) were obtained from molychem chemical reagent co. All solvents and chemicals were used without further purification.

2.2 Synthesis of MnO_2 via hydrothermal method

In a typical synthesis, 5.53 g of potassium permanganate ($KMnO_4$) and 1.27 mL of hydrochloric acid (HCl) were each dissolved separately in 70 mL of distilled water under continuous magnetic stirring to ensure homogeneity. The resulting solutions were combined and stirred thoroughly to form a uniform precursor mixture. The homogeneous solution was then transferred into a Teflon-lined stainless-steel autoclave. To prevent contamination from the top interface of the autoclave, the upper edge of the Teflon liner was sealed using polytetrafluoroethylene (PTFE) tape. The sealed autoclave was subjected to a stepwise hydrothermal treatment at 80 °C, 100 °C, and 120 °C, each for 1 h, sequentially. After the thermal treatment, the autoclave was allowed to cool naturally to room temperature. Following the reaction, the solid product (precipitated MnO_2) was carefully collected, thoroughly washed several times with deionized water to remove any residual ions or unreacted precursors, and then dried under vacuum at 40 °C for 12 h.

3. Result and discussion

3.1 XRD

The XRD patterns for the prepared MnO_2 are shown in **Fig. 1** above The XRD of MnO_2 shows the sharp & polycrystalline sample. The broad peaks are not observed. The peaks in the XRD pattern are indexed to cubic body-centred tetragonal MnO_2 structure with lattice constants of a= 1.20nm, b= 1.204nm, and C= 1.532nm. The Full Width Half Maximum (FWHM) of the sample is 0.94192°. Crystalline size using Scherrer's equation ($D = 0.9\lambda/ \beta\cos\theta$) of sample about 4.6673°. This indicates that the synthesized material is purely an individual phase without any additional second phase.

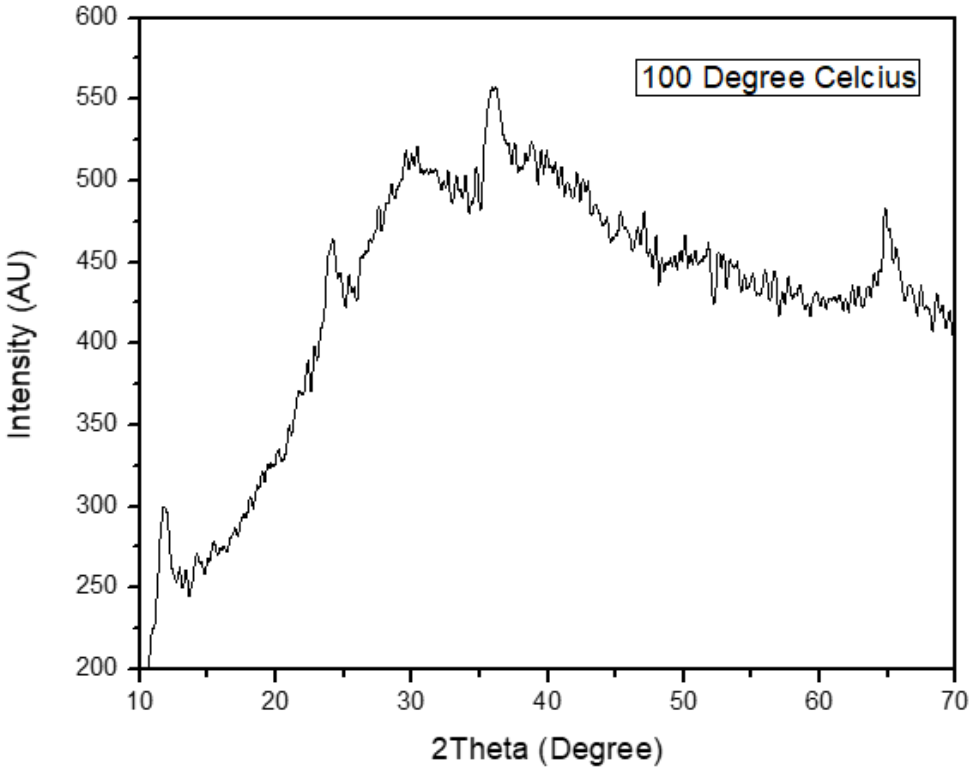

Fig. 1: X-ray diffraction pattern of nanostructured MnO_2 synthesized hydrothermally at 100° C for 1 h.

3.2 Cyclic voltammetry

The cyclic voltammetry (CV) analysis of the synthesized MnO_2 electrode is shown in **Fig. 2**. Among the samples, the MnO_2 prepared with a hydrothermal duration of 10 h exhibited the most favorable electrochemical performance, which can be attributed to its higher surface area and enhanced K^+ ion content within the structure. These characteristics contribute significantly to improved ion transport and charge storage capability. The CV curves display a quasi-rectangular shape, which is indicative of ideal capacitive behavior and excellent electrochemical reversibility. This shape reflects the electric double-layer capacitance and suggests rapid charge propagation within the MnO_2 nanowire network. However, with increasing scan rates, the CV curves begin to deviate from the ideal rectangular shape. This deviation is attributed to a reduced effective interaction between electrolyte ions and the active electrode surface at higher scan rates. As a result, the specific capacitance decreases with increasing scan rate due to limited ion diffusion and slower faradaic reaction kinetics.

The electrode composed of MnO_2 nanowires showed superior electrochemical response, suggesting that the nanowire morphology facilitates efficient ion diffusion and electron transport. This morphology enhances the utilization of the active material and supports improved capacitive performance. The specific capacitance of the MnO_2 nanowire electrode was found to be dependent on the scan rate, with higher values observed at lower scan rates. At the lowest scan rate investigated (0.01 V s^{-1}, assumed), the specific capacitance reached 1066 F g^{-1}, highlighting the excellent energy storage capability of the material.

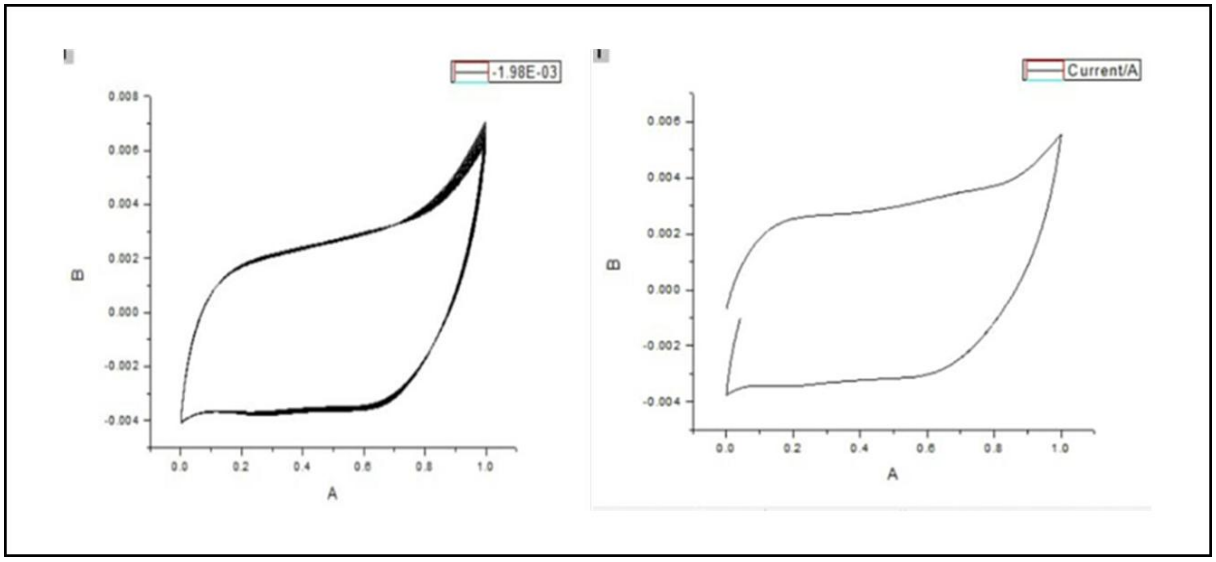

Fig. 2: Cyclic voltammetric at different scan rates form 0.01-0.09mVs^{-1}(100°c for 1hr).

3.3 Charge-discharge

The galvanostatic charge-discharge (GCD) profile of the MnO_2 nanowire electrode is presented in **Fig. 3 (a).** The GCD curves exhibit a linear and nearly symmetrical shape during both the charge and discharge processes, indicating excellent capacitive behavior and electrochemical reversibility of the electrode material. The minimal iR drop observed further supports the presence of low internal resistance and efficient charge transport within the MnO_2 nanowire structure. The applied constant current during both the charging and discharging phases was 0.001 A, and the charge/discharge times were identical at 999 seconds, suggesting good symmetry and stability of the electrode during the electrochemical process.

The charge storage mechanism is primarily governed by the intercalation and de-intercalation of cations (Na^+ and K^+) into the MnO_2 matrix. This mechanism is characteristic of pseudocapacitive behavior and contributes to the efficient storage of charge. The specific areal capacitance of the MnO_2 nanowire electrode, calculated from the discharge slope of the GCD curve, was found to be approximately 0.02724 F/cm², demonstrating its potential applicability in supercapacitor devices.

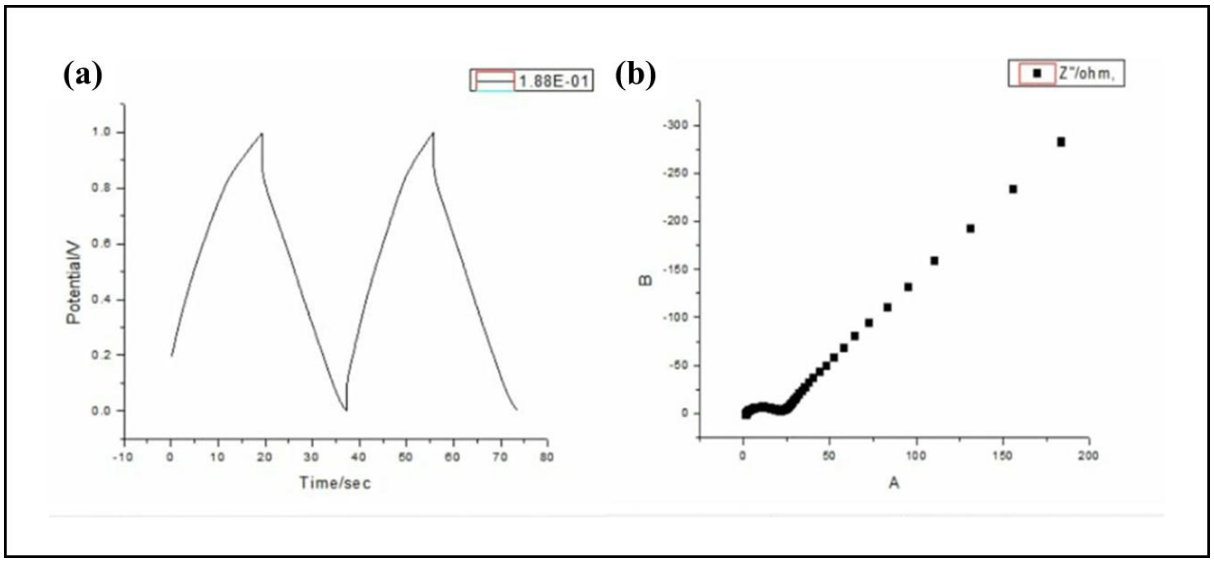

Fig. 3: (a) the galvanostatic charge-discharge curve of MnO_2 nanowires and (b) Nyquist plot for MnO_2 nanowire electrode

3.4 EIS

The electrochemical impedance spectroscopy (EIS) analysis of the MnO_2 nanowire electrode is presented in **Fig. 3 (b)**. The Nyquist plot displays a small semicircle in the high-frequency region, corresponding to a low charge transfer resistance (R_ct), followed by a straight, sloped line in the low-frequency region, which is indicative of ideal capacitive behavior. The steepness of the line in the low-frequency domain confirms efficient ion diffusion and rapid charge transport at the electrode-electrolyte interface. The low time constant, derived from the EIS data, further suggests that the MnO_2 nanowire electrode facilitates fast charge-discharge kinetics, making it a promising material for high-power supercapacitor applications. These results affirm the excellent electrochemical performance, including low internal resistance and high reversibility, of the MnO_2 nanowires as an efficient pseudocapacitive electrode material.

4. Conclusion

MnO_2 nanowires were successfully synthesized via a hydrothermal method, and their pseudocapacitive properties were studied for the first time. XRD analysis confirmed a cubic body-centered crystal structure, indicated by equal lattice parameters (a = b = c). The MnO_2 nanostructures were synthesized under varying temperatures (80 °C, 100 °C, and 120 °C) and durations, with the optimal electrochemical performance observed under specific conditions. CV analysis at a scan rate of 0.1 V/s demonstrated enhanced specific capacitance and excellent power capability, attributed to the rapid current-voltage response and good electrochemical reversibility of the MnO_2 nanowire electrode. Galvanostatic charge–discharge measurements showed symmetrical profiles with equal cathodic and anodic currents (0.001 A) and times (999 s), indicating stable capacitive behavior. EIS results further confirmed low charge transfer resistance and favorable electrochemical characteristics.

Acknowledgements

One of the authors, SSL, is grateful for financial assistance received through the Seed Money Scheme from Vivekanand College, Kolhapur (Empowered Autonomous), Ref. No. VCK/3108/2023-24 dated 30/03/2024.

5. References

1. Simon, P. and Y. Gogotsi, *Materials for electrochemical capacitors.* Nature materials, 2008. **7**(11): p. 845-854.

2. Zhang, L.L. and X. Zhao, *Carbon-based materials as supercapacitor electrodes.* Chemical society reviews, 2009. **38**(9): p. 2520-2531.

3. Conway, B.E., *Electrochemical supercapacitors: scientific fundamentals and technological applications*. 2013: Springer Science & Business Media.

4. Miller, J.R. and P. Simon, *Electrochemical capacitors for energy management.* science, 2008. **321**(5889): p. 651-652.

5. Augustyn, V., P. Simon, and B. Dunn, *Pseudocapacitive oxide materials for high-rate electrochemical energy storage.* Energy & Environmental Science, 2014. **7**(5): p. 1597-1614.

6. Lee, J.W., et al., *A facile and template-free hydrothermal synthesis of Mn3O4 nanorods on graphene sheets for supercapacitor electrodes with long cycle stability.* Chemistry of materials, 2012. **24**(6): p. 1158-1164.

7. Wang, H. and H. Dai, *Strongly coupled inorganic–nano-carbon hybrid materials for energy storage.* Chemical Society Reviews, 2013. **42**(7): p. 3088-3113.

8. Brousse, T., D. Bélanger, and J.W. Long, *To be or not to be pseudocapacitive?* Journal of The Electrochemical Society, 2015. **162**(5): p. A5185.

9. Yang, Z., et al., *Electrochemical energy storage for green grid.* Chemical reviews, 2011. **111**(5): p. 3577-3613.

10. Jiang, L.-Y., et al., *SnO2-based hierarchical nanomicrostructures: facile synthesis and their applications in gas sensors and lithium-ion batteries.* The Journal of Physical Chemistry C, 2009. **113**(32): p. 14213-14219.

11. Wang, Y., et al., *Supercapacitor devices based on graphene materials.* The Journal of Physical Chemistry C, 2009. **113**(30): p. 13103-13107.

12. Zhu, C., et al., *In situ synthesis of porous Co 3 O 4 polyhedra/carbon nanotubes heterostructures for highly efficient supercapacitors.* Ionics, 2017. **23**: p. 2175-2183.

13. Wei, W., et al., *Manganese oxide-based materials as electrochemical supercapacitor electrodes.* Chemical society reviews, 2011. **40**(3): p. 1697-1721.

14. Jiang, J., et al., *Recent advances in metal oxide-based electrode architecture design for electrochemical energy storage.* Advanced materials, 2012. **24**(38): p. 5166-5180.

15. Sun, Y., et al., *Integration of Manganese Dioxide-Based Nanomaterials for Biomedical Applications.* Advanced nanoBiomed research, 2023. **3**(1): p. 2200093.

16. Majumdar, D., *Review on current progress of MnO2-based ternary nanocomposites for supercapacitor applications.* ChemElectroChem, 2021. **8**(2): p. 291-336.

Study of graph based optimization techniques intermodal connectivity in Kolhapur's public transportation

Dr. S. P. Thorat[1] **Ms. A.D. Patil** **Ms. P.P. More**
M.Sc., M.Phil., Ph.D. M.Sc. M.Sc.

1. HOD of Department of Mathematics, Vivekanand College, Kolhapur (an Empowered Autonomous Institute), thoratsanjay15@gmail.com, 9970929595

ABSTRACT

In this paper we have to discussing the Traveling Salesman Problem (TSP) and Vehicle Routing Problem (VRP). Here we comparing the number of algorithms such as Vector Path Routing (VPR), Dijkstra's Algorithm and A* Search. And also mention the case study that is a route from the Western India Institute of Neurosciences to Aster Aadhar Hospital. By analysing multiple optimization strategies, this research aims to improve mobility, reduce travel costs, and minimize delays.

KEYWORDS : Graph, path, Traveling Salesman Problem (TSP) and Vehicle Routing Problem (VRP), Vector Path Routing (VPR), Dijkstra's Algorithm, A* Search, and Prim's Algorithm.

INTRODUCTION

The ability to travel efficiently is a crucial aspect of human activity, significantly influencing our daily lives. However, this need for mobility often leads to traffic congestion, which is a common issue that disrupts smooth travel experiences. Traffic congestion has far-reaching effects, including delays in road transportation, increased pollution levels, higher travel costs, and interruptions on routes that may seem minor. Many travellers find themselves stuck midway through their journeys, wasting valuable time and resources due to a lack of reliable and comprehensive traffic information. Anticipatory awareness of traffic conditions is essential, as it empowers individuals to select the most efficient routes available.

In logistics, transportation, and network optimization, routing challenges such as the Vehicle Routing Problem (VRP) and the Traveling Salesman Problem (TSP) present significant obstacles that need to be addressed. Effectively solving these routing problems is vital for enhancing overall productivity, reducing operational costs, and optimizing resource allocation across numerous real-world applications.

In this work we try to develop the various methods and algorithm for addressing routing transporting challenges, including A*, Dijkstra, and Bellman-Ford. These algorithms form the backbone of conventional hard computing techniques, providing predictable solutions based on strict mathematical principles. Also we study complexities of routes and routing problems within the context of road transportation systems, investigating a wide range of route optimization techniques that incorporate both soft and hard computing strategies.

PRELIMINARIES

- **Graph[8]:** A graph is formed by vertices and edges connecting the vertices. Formally, the graph is the pair of sets (V,E) is a set of edges form by Pairs of vertices.
- **Simple graph[8]:** A graph in which each edge connects two different vertices and where no two edges connect the same pair of vertices is called a simple graph.

- **Weighted Graph[8]:** Each edge has an associated weight or cost w(u ,v), which represents the cost to move from vertex u to vertex v.
- **Path[8]:** A path is a sequence of vertices connected by edges. The path cost is the sum of the weights of its edges.
- **Shortest Path[8]:** The shortest path from a source vertex s to a target vertex v is the path with the minimum total weight.
- **Path weight[8]:** The **path weight** is the sum of the edge weights in the path.
- **Cycle[8]:** A **cycle** in a graph is a path that starts and ends at the same vertex with **no repeated edges or vertices.**

MAIN RESULT

1) VRP (Vehicle Routing Problem)[9]

The concept of VRP was first introduced in 1956 by researchers Ramser and Dantzig, who developed strategies to optimize gasoline supply routes. This marked the beginning of mathematical approaches to solving routing issues. The main aim of the VRP is to reduce the total transportation costs. This includes minimizing the distance travelled by the vehicles and ensuring that each client is served efficiently, ideally only once.

Algorithm for VPR (Vector Path Routing)[9]

Step 1: Identify key- places (nodes) along the route.

Step 2: Draw a graph – For representing nodes and the distances between them.

Step 3: Apply VPR formula-

Cost (u ,v) = d(u, v) + h(v)

Where, d(u ,v) = distance between nodes u and v.

h(v)= heuristic estimate (we can assume it to be straight-line distance to end node)

assume, h(v)= 0.

Step 4: Finally got Shortest Path between different nodes.

2) TSP (Travelling Salesman Problem)[7]

The Traveling Salesman Problem (TSP) revolves around finding the optimal path for a salesperson, starting from a specified origin, visiting multiple locations in sequence, and returning to the starting point. Key points include:

Algorithm for TSP (Travelling Salesman Problem)[7]

Step 1: Select 6 Key Locations (Nodes)

Step 2: Draw the distance Table

Step 3: apply the TSP Formula

$$\text{TSP}_{\text{total}} = \min_{\text{permutations}} \sum_{i=1}^{n} d(p_i, p_{i+1}) + d(p_n, p_1)$$

Step 4: Got the final result (Min Distance).

3) Dijkstra's algorithm[10]

Dijkstra's algorithm is a way to find the shortest path between two points in a network, like a map with cities or a metro system with stations. It works step by step to figure out the quickest route from the starting point to the destination.

Algorithm for Dijkstra's algorithm

Step 1: Define Nodes (Places on Map)

Step 2: Draw the distance Table (Weighted Graph in km, approximated)

Step 3: Apply the Dijkstra's Algorithm Formula

Initialize distances:

dist[source]=0, dist[others]=∞

Update neighbours:

dist[v]=min(dist[v],dist[u]+weight(u,v))

Step 4: Got the final result (shortest distance)

4) ALT (A* search Landmarks and Triangle inequality)[10]

The ALT algorithm is a pre-processing method aimed at optimizing Dijkstra's algorithm for computing shortest paths in extensive road networks by selecting specific nodes known as landmarks for faster computations. A* is a search algorithm that finds the least-cost path from a start node to a goal node, using a cost function that combines:

Algorithm for A* algorithm

Step 1: Define Nodes (Places)

Step 2: Distance Table (g(n), estimated in km)

Step 3: Heuristic Table (h(n), estimated straight-line distance to F)

Step 4: A* Search (f(n) = g(n) + h(n))

g(n): Cost from start node to current node

h(n): Heuristic (estimated cost from current node to goal)

f(n): Total estimated cost of the path through node n

Step 5: Got the final result.

***Discussion and Comparison between different algorithms:**

Here we find the best (shortest) path from western India Institute of neurosciences to Aster Aadhar Hospital in Kolhapur by using above the all algorithms.

Node	Location
A	Western India Institute (Start)
B	Mahavir College Chowk
C	Shahupuri
D	Sayaji Hotel
E	Tarabai Park
F	Aster Aadhar Hospital (End)

Method	Path	Shortest distance
VPR (Vector Path Routing)	A-B-D-E-F	4.7
TSP(Travelling Salesman Problem)	A-B-C-D-E-F-A	9.4
Dijkstra's Algorithm	A-B-C-D-E-F	5.4
A* Algorithm	A-B-C-D-E-F	5.4

CONCLUSION

We find the best (shortest) path from western India Institute of neurosciences to Aster Aadhar Hospital in Kolhapur by using VPR (Vector Path Routing). Also we observe that VPR (Vector Path Routing) method gives the shortest path and TSP(Travelling Salesman Problem) method gives largest path but its starting and end point are same. Both Dijkstra's algorithm and the A* algorithm are widely used for finding the shortest paths in graphs, but they differ in efficiency, applicability, and overall effectiveness.

REFERENCES

1. C.T. Liu: Discrete Mathematics.
2. Evans A.G., Hutchinson J.W. Ashby M.F., (1998) Multifunctionality of cellular metal systems, Prog. Mater. Sci., 43, 171–221.
3. Gibson, L.J. (1989) Modelling the mechanical behaviour of cellular materials. Mater.Sci. Eng. A 110, 1–36.
4. Gibson, L.J.; Ashby, M.F. (1997) Cellular Solids: Structure and Properties, 2nd ed.; Cambridge University Press: Cambridge, UK, 16–21.
5. Gorrett Birkhoff: Lattice Theory 2. Rich and Brualdi: Combinatoric.
6. Ian P. Gent, Toby Walsh (1996) "The TSP phase transition" Artificial Intelligence ,88, 349-358.
7. John Clark and Derek Holton, (1991) "A first look at graph Theory" Allied Publishers Ltd.

8. Niklas Kohl, Oli B. G. Madsen, (1997) "An Optimization Algorithm for the Vehicle Routing Problem with Time Windows Based on Lagrangian Relaxation" Operations Research 45(3):395. https://doi.org/10.1287/opre.45.3.395

9. Ritik Gupta, Isha, Gunjan Aggarwal, (2024)"Effective Route Optimization: A Comparative Study of Algorithms and Techniques" International Conference on Innovative Computing & Communication (ICICC).

10. Symon Lipschitz and Mark Lipson: Discrete Mathematics (second edition), Tata McGraw hill Publishing Company Ltd. New Delhi.

A Simple Dip Coating Approach for Superhydrophobic TiO_2/Polystyrene Nanocomposite Coatings with Self-Cleaning Application

Rutuja A. Ekunde[1], Rajaram S. Sutar[2], Pradip P. Gaikwad[1], Sagar S. Ingole[1], Akshay R. Jundle[1], Sanjay S. Latthe[1]*

[1] Self-cleaning Research Laboratory, Department of Physics, Vivekanand College, Kolhapur (An Empowered Autonomous Institute), (Affiliated to Shivaji University, Kolhapur), Kolhapur – 416003, Maharashtra, India.

[2] School of Chemistry and Molecular Sciences, Henan University, Kaifeng, China.

*Corresponding author E-mail: latthes@gmail.com

Abstract

This study presents a facile and cost-effective strategy for fabricating superhydrophobic coatings using hydrothermally synthesized titanium dioxide (TiO_2) nanoparticles. TiO_2 nanoparticles were prepared via a hydrothermal method. A dip-coating technique was used to deposit the superhydrophobic layer on pre-cleaned glass substrates. The coating solution was formulated by dispersing unmodified TiO_2 nanoparticles in a polymethylhydrosiloxane (PMHS) and chloroform mixture, with polystyrene (PS) added as a binder to improve film uniformity and adhesion. The coating exhibited the highest superhydrophobic performance, achieving a static water contact angle of 164° and a sliding angle of 5°, indicating excellent water repellency. The mechanical robustness of the coated glass slide was evaluated through a muddy water resistance test. The prepared superhydrophobic coating revealed excellent self-cleaning performance against the muddy water. The developed coatings hold significant potential for applications in self-cleaning due to their simplicity, scalability, and superhydrophobic behavior.

Keywords: Superhydrophobic, TiO_2 nanoparticles, dip coating, self-cleaning

1. Introduction

Superhydrophobic surfaces have garnered significant interest due to their remarkable water-repellent property, which makes them ideal for preventing the accumulation of dirt [1]. Inspired by natural surfaces such as lotus leaves, which exhibit unique self-cleaning properties. The superhydrophobic surface is defined by its wetting character, which shows a static water contact angle (WCA) greater than 150° and a sliding angle (SA) smaller than 10° [2]. The superhydrophobicity on the lotus leaf surface occurs due to a thin waxy layer on micro-scale papillae [3]. Various strategies have been employed to fabricate such surfaces, primarily by introducing surface roughness and incorporating low surface energy materials [4]. Numerous bioinspired and synthetic approaches have been explored to develop multifunctional surfaces with micro/nano features for applications including self-cleaning [5], oil–water separation [6], corrosion protection [7], anti-icing [8] and etc. In previous studies, a wide range of materials including SiO_2, TiO_2, ZnO, Al_2O_3, candle soot, and various polymers, have been employed in the development of self-cleaning superhydrophobic coatings. Latthe et al. [2] applied a suspension of hydrophobic SiO_2 nanoparticles (NPs) to various substrates, including motorcycle bodies, building walls, mini boats, solar cell panels, window glass, cotton shirts, fabric shoes, cellulose paper, metal, wood, sponges, plastic, and marble. These coatings demonstrated excellent water repellency and outstanding self-cleaning properties. Ding et al. [9] developed a superhydrophobic fluorinated polysiloxane/TiO_2 nanocomposite coating applicable to substrates such as aluminum, glass, wood, paper, and polypropylene. The coating exhibited excellent durability across a wide pH range, varying temperatures, and UV exposure, and was recoverable after oil contamination. A FAS-TiO_2/PVDF composite formed hierarchical micro/nanostructures via electrostatic interactions, and when applied to a copper substrate, showed a water contact angle of 160° and a sliding angle of 5°. Kokare et al.

[10] developed a self-cleaning superhydrophobic coating using Octadecyltrichlorosilane(ODS)-modified TiO_2 nanoparticles through a dip coating method. TiO_2 nanoparticles were dispersed in ethanol with varying concentrations of ODS to enhance hydrophobicity. The coatings prepared with five deposition layers exhibited a water contact angle above 150° and a sliding angle below 10°. Increasing ODS concentration improved surface roughness, enhancing water repellency. The coatings demonstrated stability against water jet impact and effectively repelled colored and muddy water, making them suitable for self-cleaning applications. In this work, TiO_2 nanoparticles were synthesized via a hydrothermal method and utilized to fabricate a superhydrophobic coating through a simple dip coating process. The coating was developed by incorporating PMHS and PS as surface-modifying and binding agents. The influence of coating thickness was investigated by varying the number of dip-coating cycles. The coating shows excellent superhydrophobicity and self-cleaning performance. This facile approach offers a cost-effective route to prepare superhydrophobic coating with potential applications in self-cleaning technologies.

2. Experimental Section

2.1 Chemicals

Titanium tetraisopropoxide (TTIP) was procured from Spectrochem Pvt. Ltd., Mumbai, India. Polymethylhydrosiloxane (PMHS) and polystyrene (PS) were purchased from Sigma Aldrich. Ethanol, Chloroform ($CHCl_3$) were procured from Loba Chemie. Micro glass substrates (75× 25 × 1.35 mm) were obtained from Blue star, Polar Industrial Corporation, India.

2.2 Synthesis of TiO_2 Nanoparticles via Hydrothermal Method

Initially, 20 mL of ethanol was mixed with 30 mL of distilled water and stirred at 400 rpm for 20 min to form a homogeneous solution. Subsequently, 15 mL of titanium tetraisopropoxide (TTIP) dissolved in 25 mL of ethanol was added dropwise to the above mixture under continuous stirring. The resulting sol was further stirred at ambient temperature for 2 h to promote hydrolysis and condensation reactions, forming a uniform sol-gel system. The obtained sol-gel was transferred to a Teflon-lined stainless-steel autoclave and subjected to hydrothermal treatment at 80 °C for 24 h. Upon completion, the product was collected and dried at 40 °C for 3 h to remove residual solvents. The dried material was ground using an agate mortar to reduce particle size and improve uniformity. Finally, the resulting powder was calcinated at 400 °C for 2 h to obtain TiO_2 nanoparticles.

2.3.Preparation of TiO_2-PS Superhydrophobic Coating

The glass substrates were sequentially cleaned using ultrasonic treatment in 0.1 M Hcl, 0.1 M NH_4OH, ethanol, and distilled water, each for 10 minutes. After cleaning, the substrates were dried in a hot air oven at 60 °C for 10 minutes before being utilized for the fabrication process. Initially by dissolving 0.16 mL of PMHS in 40 mL of chloroform. The mixture was stirred for 20 min using a magnetic stirrer at 100 rpm to ensure complete dissolution. Subsequently, 800 mg of unmodified TiO_2 nanoparticles were added to the PMHS solution, and the resulting suspension was stirred continuously for 1 h to achieve a homogeneous dispersion of nanoparticles. Simultaneously, in a separate beaker, 200 mg of PS was dissolved in 20 mL of chloroform. This PS solution was then added to the TiO_2-PMHS suspension under constant stirring. The combined mixture was stirred for an additional 30 min to obtain a uniform and stable coating solution suitable for deposition. Pre-cleaned glass slides were immersed in the prepared coating solution. The number of deposition cycles was varied as 1, 2, and 3, respectively, to study the influence of coating thickness. After deposition, the coated slides were dried in an oven at 100 °C for 30 min to ensure solvent evaporation and film formation.

3. Results and Discussion

3.1. Wettability

The wettability of the fabricated superhydrophobic glass surfaces was assessed by measuring the water contact angle using a contact angle goniometer. Samples were prepared with one, two, and three deposition cycles to evaluate the effect of deposition frequency on surface hydrophobicity. The results showed a clear trend of increasing WCA with the number of deposition cycles, indicating enhanced surface superhydrophobicity. Specifically, the WCA for the sample with one deposition cycle was measured at 154°, which increased to 159° after two deposition cycles. Further improvement was observed with three deposition cycles, where the WCA reached 164°. This progressive increase in WCA demonstrates that a greater number of deposition cycles contributes to the development of hierarchical surface roughness and reduced surface energy, two critical factors for achieving superhydrophobic behavior. Therefore, the surface coated with three deposition cycles exhibited the highest degree of water repellency, representing the optimal condition for superhydrophobic performance in this study.

3.2. Self-Cleaning Ability

The self-cleaning ability of the superhydrophobic coating was tested using a simple muddy water test. A stream of muddy water was poured onto the coated glass slide to observe its behaviour.

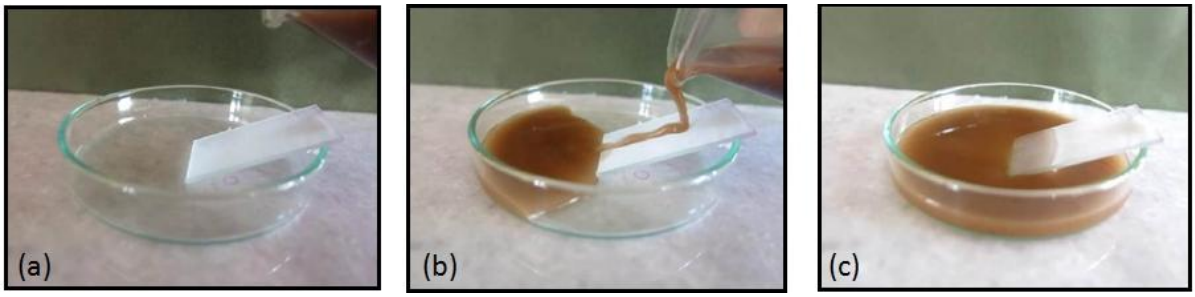

Fig. 1: Photograph showing muddy water rolling off the coated glass slide during the self-cleaning performance.

The muddy water was seen to roll off the surface without leaving any residues, indicating excellent self-cleaning performance. This property is attributed to the high water contact angle and low surface adhesion of the superhydrophobic surface.

3.3. Mechanical Durability

The mechanical durability of superhydrophobic coatings is a critical factor for their real-world applicability, particularly in outdoor environments where surfaces may be subjected to physical wear and environmental contaminants. In this study, the mechanical robustness of the coated glass slide was evaluated through a muddy water resistance test. Approximately 2 L of muddy water were continuously poured over the coated surface to simulate prolonged exposure to abrasive and wet conditions. Prior to the test, the WCA of the coated slide was measured at 164°, indicating excellent superhydrophobicity. However, after the durability test, a noticeable reduction in WCA was observed, decreasing to 154°, which suggests partial degradation of the surface coating due to mechanical stress. Despite this reduction, the surface maintained a contact angle above 150°, confirming that the coating still exhibited superhydrophobic behavior. These results indicate that while some loss in hydrophobic performance occurred, the coating retained moderate mechanical durability under harsh testing conditions.

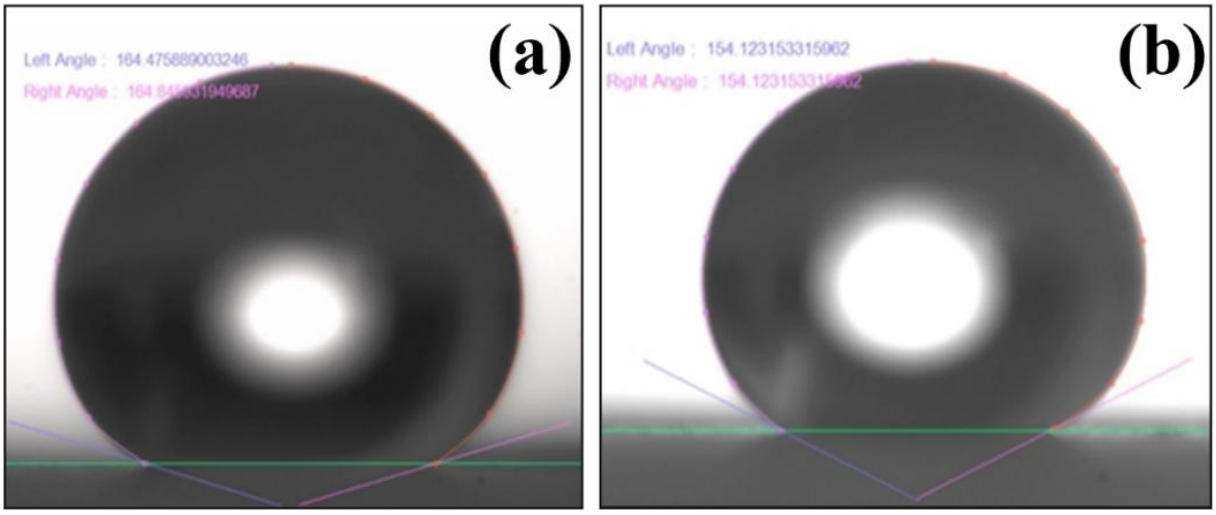

Fig. 2: Water contact angle of the coating (a) before durability test (164 °) and (b) after durability test (154°).

4. Conclusion

We have successfully fabricated superhydrophobic surface on a glass substrate using the simple dip coating technique. The method employed a mixture of PMHS, chloroform, and TiO_2 nanoparticles. The fabricated surface exhibited a water contact angle of up to 164° and a sliding angle of 5°. The coated glass slides demonstrated excellent self-cleaning behavior by repelling muddy water without residue. Moreover, the coating retained its superhydrophobic nature even after a mechanical durability test involving muddy water, although a slight reduction in contact angle was noted. Overall, the dip coating technique proved to be a simple and effective method for fabricating superhydrophobic coatings with promising practical applications.

Acknowledgements

One of the authors, SSL, is grateful for financial assistance received through the Seed Money Scheme from Vivekanand College, Kolhapur (Empowered Autonomous), Ref. No. VCK/3108/2023-24 dated 30/03/2024.

References:

[1] S. Wang, K. Liu, X. Yao, L. Jiang, Bioinspired surfaces with superwettability: new insight on theory, design, and applications, Chemical reviews, 115 (2015) 8230-8293.

[2] S.S. Latthe, R.S. Sutar, V.S. Kodag, A. Bhosale, A.M. Kumar, K.K. Sadasivuni, R. Xing, S. Liu, Self–cleaning superhydrophobic coatings: Potential industrial applications, Progress in Organic Coatings, 128 (2019) 52-58.

[3] Z. Liang, M. Geng, B. Dong, L. Zhao, S. Wang, Transparent and robust SiO2/PDMS composite coatings with self-cleaning, Surface Engineering, 36 (2020) 643-650.

[4] S.S. Latthe, C. Terashima, K. Nakata, M. Sakai, A. Fujishima, Development of sol–gel processed semi-transparent and self-cleaning superhydrophobic coatings, Journal of Materials Chemistry A, 2 (2014) 5548-5553.

[5] X. Wang, H. Ding, S. Sun, H. Zhang, R. Zhou, Y. Li, Y. Liang, J. Wang, Preparation of a temperature-sensitive superhydrophobic self-cleaning SiO2-TiO2@ PDMS coating with photocatalytic activity, Surface and Coatings Technology, 408 (2021) 126853.

[6] P. Xu, X. Li, Fabrication of TiO2/SiO2 superhydrophobic coating for efficient oil/water separation, Journal of Environmental Chemical Engineering, 9 (2021) 105538.

[7] X. Liu, T. Zhan, B. Zhang, Attapulgite-based superhydrophobic coating on aluminum alloy substrate with self-cleaning, anti-corrosion and robustness, Journal of Industrial and Engineering Chemistry, 130 (2024) 357-367.

[8] X. Zhou, S. Yu, S. Jiao, Z. Lv, E. Liu, Y. Zhao, N. Cao, Fabrication of superhydrophobic TiO2 quadrangular nanorod film with self-cleaning, anti-icing properties, Ceramics International, 45 (2019) 11508-11516.

[9] X. Ding, S. Zhou, G. Gu, L. Wu, A facile and large-area fabrication method of superhydrophobic self-cleaning fluorinated polysiloxane/TiO 2 nanocomposite coatings with long-term durability, Journal of Materials Chemistry, 21 (2011) 6161-6164.

[10] A.M. Kokare, R.S. Sutar, S. Deshmukh, R. Xing, S. Liu, S.S. Latthe, ODS–modified TiO2 nanoparticles for the preparation of self-cleaning superhydrophobic coating, in: AIP Conference Proceedings, AIP Publishing, 2018.

Fabrication of Silica-PS Self-cleaning Superhydrophobic Coating on Glass Substrate

Sagar S. Ingole[1], Rajaram S. Sutar[2], Pradip P. Gaikwad[1], Akshay R. Jundle[1], Rutuja A. Ekunde[1], Sanjay S. Latthe[1]*

[1] Self-cleaning Research Laboratory, Department of Physics, Vivekanand College, Kolhapur (An Empowered Autonomous Institute), (Affiliated to Shivaji University, Kolhapur), Kolhapur – 416003, Maharashtra, India.
[2] School of Chemistry and Molecular Sciences, Henan University, Kaifeng, China.
*Corresponding author E-mail: latthes@gmail.com

Abstract

In this study, a superhydrophobic coating was fabricated by spray-depositing a composite solution of Polystyrene (PS) and Methyltrichlorosilane (MTCS)-modified silica nanoparticles onto glass substrates. Initially, silica nanoparticles were synthesized via a sol-gel process in a basic condition using tetraethyl orthosilicate (TEOS) as the precursor. The resulting particles were subsequently functionalized with MTCS to introduce low-surface-energy methyl groups. These modified nanoparticles were then dispersed in a PS solution to formulate a sprayable suspension. Upon deposition and drying, the coated glass surfaces exhibited a high-water contact angle of 166°, indicating excellent superhydrophobicity. Furthermore, the coating demonstrated outstanding water jet impact resistance, highlighting its mechanical and chemical stability and potential for real-world self-cleaning applications.

Keywords: Superhydrophobic, silica coating, spray coating, self-cleaning

1. Introduction

Self-cleaning superhydrophobic coatings have attracted considerable scientific interest due to their exceptional water-repellent performance across a variety of substrates. Inspired by natural examples such as lotus leaves and insect wings, these coatings achieve their functionality through the integration of micro- and nanoscale surface textures with materials of inherently low surface energy. Superhydrophobicity is typically characterized by a water contact angle exceeding 150° and low contact angle hysteresis, enabling water droplets to bead up and roll off the surface effortlessly, removing dust and other contaminants in the process. This behavior is primarily governed by the synergy between surface roughness at multiple length scales and chemical modifications that reduce adhesion between water and the surface [1]. Achieving superhydrophobicity relies heavily on the presence of surface roughness. The Wenzel and Cassie-Baxter models explain how surface texture influences wettability, either enhancing or reducing it depending on the interaction between the liquid and the rough features. Superhydrophobic behavior is typically associated with the Cassie-Baxter state, where air pockets remain trapped beneath the water droplet, minimizing solid–liquid contact. This effect is most effectively achieved on hierarchical surfaces, where microscale structures are further decorated with nanoscale features. To complement this surface architecture, materials with inherently low surface energy such as fluorinated compounds or silicones are often used, as they reduce the attraction between water molecules and the surface, thereby enhance the water-repellent properties [2]. Because of their very special properties, superhydrophobic coatings have very broad applications. Notably, in self-cleaning surfaces, droplets roll off and take out dirt and contaminants [3].

Darmawan et al. [4] developed a thin hydrophobic silica layer by varying the concentration of the TMCS and TEOS precursors. This study reported that, higher concentration leads to elevation in WCA. Also, decrease trend in WCA was observed by elevating the calcination temperature. Kurbanova et al. [5] fabricated superhydrophobic coating of SiO_2/TMCS via spray deposition for self-cleaning application. The

coating exhibited high WCA of 165° with SA less than 10° which showed excellent self-cleaning ability against sands during self-cleaning performance. Sutar et al. [6] developed PS/OTS coating on SS mesh to achieve superhydrophobic attributions via dip coating method. The consecutive layers of PS and OTS was able to generate hierarchical rough structure which exhibited high WCA of 157.5 ± 2° and SA of 6 ± 2°. In the present study, we have prepared a superhydrophobic coating on a glass substrate via facile spray coating technique. In a composite solution of TMCS modified silica particles and PS prepared sample exhibited high water contact angle of 166° and SA of less than 5°. Furthermore, to access the durability of the coating various mechanical and chemical tests were performed.

2. Experimental

2.1 Materials

Polystyrene (PS, Mw ~ 280000), Tetraethylorthosilicate (TEOS, 98%) and Trimethylchlorosilane (TMCS) were purchased from Sigma Aldrich. Hexane, toluene, ammonia solution (NH_4OH – 25%), ethanol (99.9%) was procured from Loba Chemie. Glass slides (CAT. No. 72900135) was obtained from Riveria, India.

2.2 Preparation of hydrophobic silica nanoparticles

In 20 mL of ethanol, 5 mL of distilled water and 4 mL of TEOS were added. This solution was stirred about 20 min then 5 mL of NH_4OH was added and stirring continued for 6 h. The white solution then aged overnight. The dried solution was ground to earn fine silica particles. The grounded silica nanoparticles were added in the 10 v/v% TMCS-Hexane solution and stirred for 2 h at 60 ℃. Finally, these silica nanoparticles were grounded to earn hydrophobic silica nanoparticles.

2.3 Fabrication of superhydrophobic coating

A 16 mg PS was dissolved in 20 mL of toluene by stirring for 30 min. Then 200 mg as prepared silica particles were added in PS solution and further stirred for 30 min. The final solution was sprayed on clean glass substrate from a distance of 10 cm at a pressure of 2 bar. Finally, the spray coated glass samples dried at 100 ℃ for 1 h.

3. Results and discussion

Silica nanoparticles were successfully synthesized using the sol-gel method under basic conditions by utilising TEOS as the silica precursor. The alkaline environment facilitated controlled hydrolysis and condensation, yielding silica nanoparticles. These nanoparticles were subsequently modified using methyltrichlorosilane (MTCS), which reacts with surface silanol groups to introduce hydrophobic methyl (-CH_3) functionalities. The MTCS modification not only reduces the surface energy of the silica particles but also enhances compatibility with the hydrophobic polymer matrix of polystyrene. the sprayed coating formed a hierarchical surface topology. The micro/nanostructured roughness was generated by the random stacking of MTCS-modified silica nanoparticles embedded within the polystyrene matrix. This dual-scale roughness is essential for achieving the Cassie-Baxter wetting state, which traps air and minimizes water-solid contact.

The water contact angle (WCA) measured on the coated glass surface was found to be 166°, indicating outstanding superhydrophobicity. The high contact angle can be attributed to the synergistic effect of the low-surface-energy MTCS groups and the hierarchical roughness imparted by the silica nanoparticles. The sliding angle (SA) was observed to be below 5°, demonstrating excellent water repellency and low adhesion, allowing water droplets to easily roll off the surface. To evaluate the mechanical robustness of the coating, a

water jet impact test was performed. The superhydrophobic surface retained its high contact angle and low sliding angle even after continuous exposure to a high-velocity water stream for several minutes. This indicates strong adhesion of the coating to the substrate and mechanical stability of the hierarchical surface features. The success in withstanding water jet impact demonstrates the potential application of this coating in real-world self-cleaning environments, where exposure to rain, spray, or washing is common.

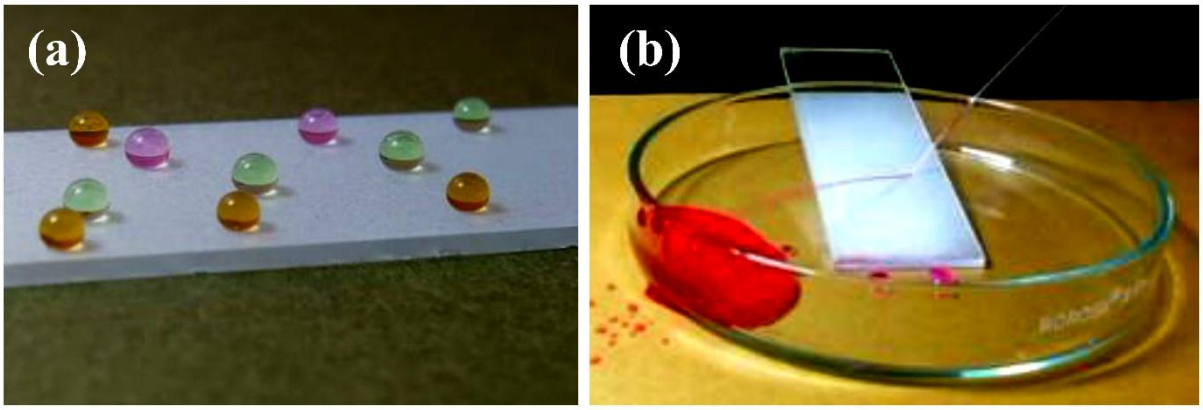

Figure 1. An optical image of (a) different colour water droplets and (b) water jet impact test on superhydrophobic sample.

To evaluate the mechanical and chemical robustness of the superhydrophobic glass samples, a series of durability tests were performed. The variation in water contact angle (WCA) was recorded as a measure of surface wettability. The adhesive tape peeling test (Figure 2a) was conducted to assess the mechanical adhesion and robustness of the coating under repetitive stress. The initial WCA of the pristine surface was 166°, indicating excellent superhydrophobicity. However, with each successive peeling cycle, the contact angle showed a gradual decline. After four tape peelings, the WCA dropped to around 91.2°, suggesting partial removal or deformation of the hierarchical surface structure responsible for hydrophobicity. In the sandpaper abrasion test (Figure 2b), the coated glass substrate was dragged over a standardized abrasive surface to simulate physical wear. The WCA decreased steadily from 166° to about 98° as the total dragging distance increased from 0 to 60 cm. This behavior confirms that abrasion deteriorates the surface texture, thereby reducing the air-trapping ability essential for sustaining superhydrophobicity. While the coating retained some hydrophobic character.

To further assess durability under fluid interaction, a water impact test was performed by continuously pouring water over the surface (Figure 2c). The contact angle remained relatively stable up to 400 mL of water but then exhibited a noticeable decline, reaching 112.4° after exposure to 1000 mL of water. This drop reflects partial damage to the micro/nanoscale roughness or possible leaching of the hydrophobic components, highlighting that prolonged exposure to dynamic water flow can compromise the superhydrophobic performance. In contrast, the coating demonstrated excellent chemical stability when exposed to aqueous water droplets of varying pH values ranging from 2 to 12 (Figure 2d). The WCA remained consistently high across the entire pH range, varying only slightly between 165° and 172°. This indicates that the surface chemistry of the coating is resistant to acidic and basic environments, thereby confirming the chemical robustness of the MTCS-polystyrene-based system.

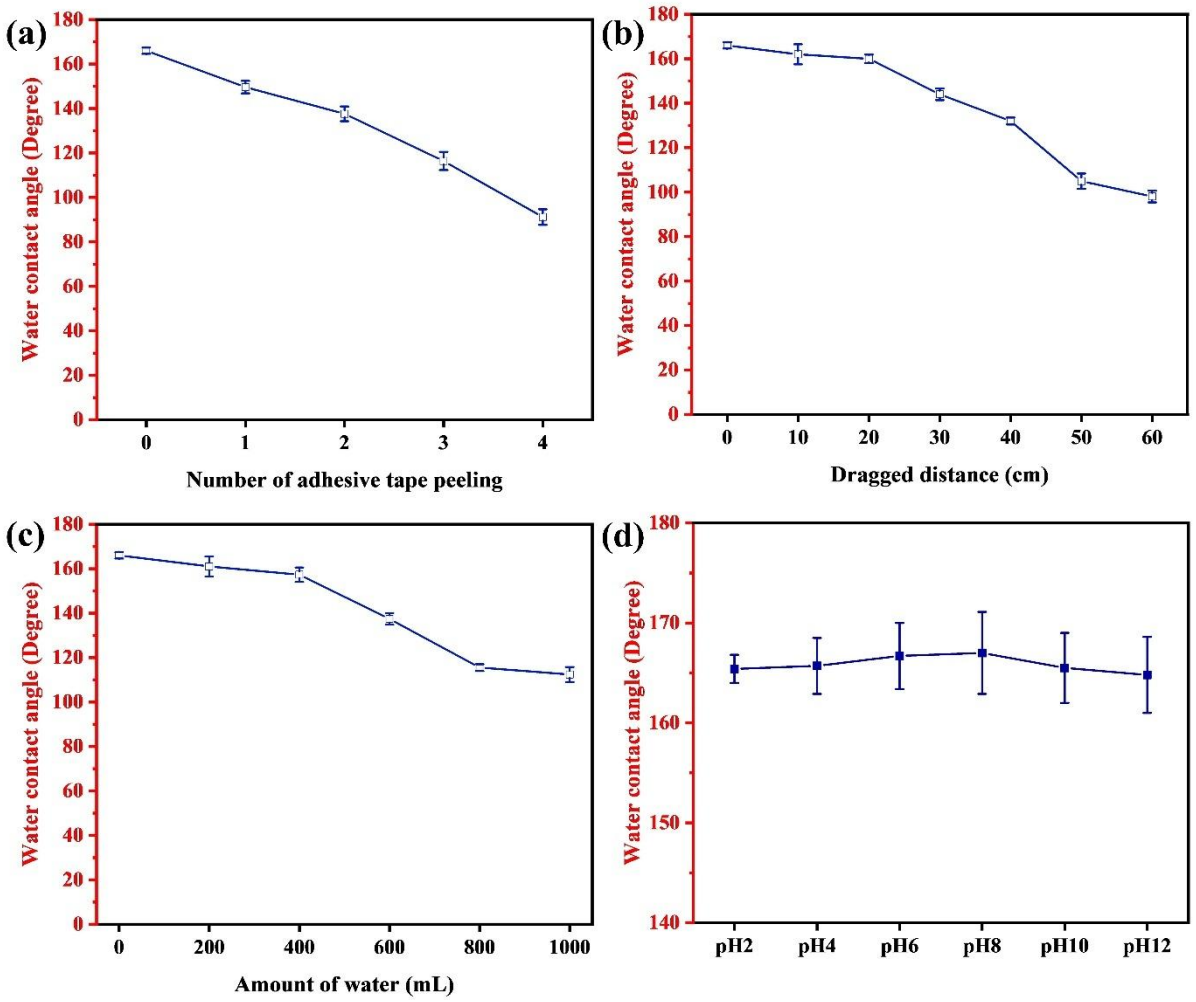

Figure 2. Water contact angle variations under (a) adhesive tape test, (b) sandpaper abrasion test, (c) water droplet impact and (d) different pH water droplets of the superhydrophobic coating.

4. Conclusion

This study reports a superhydrophobic coating by spraying a mixture of MTCS-modified silica nanoparticles and polystyrene onto glass. The surface showed excellent water repellency, with a contact angle of 166°, and stayed highly water-resistant even under strong water jet impact. Furthermore, the prepared sample exhibited good stability under mechanical tests such as adhesive tape test, sandpaper abrasion test and water droplet impact test. Also, excellent resistance to different pH water droplets. Therefore, this simple spray-based coating holds strong potential for real-world applications like self-cleaning glass.

Acknowledgements

One of the authors, SSL, is grateful for financial assistance received through the Seed Money Scheme from Vivekanand College, Kolhapur (Empowered Autonomous), Ref. No. VCK/3108/2023-24 dated 30/03/2024.

References

[1] D.M. Spori, T. Drobek, S. Zürcher, M. Ochsner, C. Sprecher, A. Mühlebach, N.D. Spencer, Beyond the lotus effect: roughness influences on wetting over a wide surface-energy range, Langmuir, 24 (2008) 5411-5417.

[2] N. Abu Jarad, H. Imran, S.M. Imani, T.F. Didar, L. Soleymani, Fabrication of superamphiphobic surfaces via spray coating; a review, Advanced Materials Technologies, 7 (2022) 2101702.

[3] M.A. Sarshar, D. Song, C. Swarctz, J. Lee, C.-H. Choi, Anti-icing or deicing: Icephobicities of superhydrophobic surfaces with hierarchical structures, Langmuir, 34 (2018) 13821-13827.

[4] A. Darmawan, S.A. Rasyid, Y. Astuti, Modification of the glass surface with hydrophobic silica thin layers using tetraethylorthosilicate (TEOS) and trimethylchlorosilane (TMCS) precursors, Surface and Interface Analysis, 53 (2021) 305-313.

[5] A. Kurbanova, N. Myrzakhmetova, N. Akimbayeva, K. Kishibayev, M. Nurbekova, Y. Kanagat, A. Tursynova, T. Zhunussova, A. Seralin, R. Kudaibergenova, Superhydrophobic SiO2/trimethylchlorosilane coating for self-cleaning application of construction materials, Coatings, 12 (2022) 1422.

[6] R.S. Sutar, S.S. Latthe, N.B. Gharge, P.P. Gaikwad, A.R. Jundle, S.S. Ingole, R.A. Ekunde, S. Nagappan, K.H. Park, A.K. Bhosale, Facile approach to fabricate a high-performance superhydrophobic PS/OTS modified SS mesh for oil-water separation, Colloids and Surfaces A: Physicochemical and Engineering Aspects, 657 (2023) 130561.

दक्षिण महाराष्ट्रातील निवडक जैन व्यक्तिमत्वांचा ऐतिहासिक आढावा.

श्री. सुरज विजय चौगुले*
शोध विद्यार्थी,
इतिहास विभाग,
शिवाजी विद्यापीठ, कोल्हापूर

डॉ. एस.आर. कट्टीमनी **
संशोधक गाईड,
विवेकानंद कॉलेज, कोल्हापूर

घोषवारा:

दक्षिण महाराष्ट्र हा ऐतिहासिक, सांस्कृतिक आणि सामाजिकदृष्ट्या समृद्ध असा प्रदेश आहे. या भूभागाला जैन धर्माचा हजारो वर्षांचा वैभवशाली वारसा लाभलेला आहे. जैन धर्म हा भारतातील एक प्राचीन धर्म असून, तो लोकशाही मूल्यांवर आधारित समता, अहिंसा आणि सहिष्णुतेचा पुरस्कार करतो. महाराष्ट्रातील जैन समाज केवळ धार्मिकच नव्हे, तर सामाजिक, शैक्षणिक, आर्थिक, सांस्कृतिक आणि औद्योगिक क्षेत्रांतही अग्रगण्य राहिला आहे. विशेषतः कोल्हापूर, सांगली, सोलापूर, रत्नागिरी आणि सिंधुदुर्ग या जिल्ह्यांमध्ये जैन समाजाने समाजाच्या सर्वांगीण विकासात मोलाची भूमिका बजावली आहे.

महाराष्ट्रातील जैन समाजाची ओळख केवळ 'गुजराती-मारवाडी व्यापारी' अशी मर्यादित न ठेवता, तो मराठी भाषिक, स्थानिक आणि दिगंबर परंपरेचा वारसा जपणारा एक महत्त्वाचा समाज घटक म्हणूनही ओळखला जातो. चतुर्थ, पंचम, सैतवाल, कासार अशा विविध जातीय घटकांमधून जैन समाजाने आपली स्वतंत्र ओळख निर्माण केली आहे. जैन कासार समाज, सैतवाल समाज, पंचम समाज, तसेच श्वेतांबर आणि दिगंबर परंपरेतील विविध संघटना, संस्था आणि व्यक्तिमत्त्वे यांनी समाजाच्या संघटन, धर्मप्रसार, शिक्षण, आरोग्य, उद्योग, कला, साहित्य आणि सामाजिक सुधारणांमध्ये मोठे योगदान दिले आहे.

संज्ञा पारिभाषिक शब्द: दक्षिण महाराष्ट्र, लोकशाही, अहिंसा, सहिष्णुता, श्वेतांबर, दिगंबर

प्रस्तावना:

दक्षिण महाराष्ट्रातील जैन समाजाच्या इतिहासाचा मागोवा घेतल्यास, प्राचीन काळापासून या समाजाने महाराष्ट्राच्या सांस्कृतिक आणि सामाजिक जीवनावर आपला ठसा उमटवला आहे. प्राचीन मराठी भाषेतील पहिले शिलालेख, साहित्यनिर्मिती, स्थापत्यकला, भव्य मंदिरे, गुंफा, पाणी व्यवस्थापनाची सोय, शिक्षणसंस्था, धर्मशाळा, तसेच विविध सामाजिक उपक्रम यामध्ये जैन समाजाचा मोठा वाटा आहे. जैन कासार समाज, पंचम समाज, सैतवाल समाज आणि इतर घटकांनी महाराष्ट्राच्या ग्रामीण आणि शहरी दोन्ही भागांत आपली सामाजिक बांधिलकी सातत्याने जपली आहे. 'जैन कासार समाज संस्था', 'दक्षिण भारत जैन सभा', 'जैन कासार समाचार' मासिक, विविध धर्मशाळा, शैक्षणिक संस्था, महिला संघटना, युवक मंडळे, तसेच अनेक सेवाभावी संस्था यांद्वारे समाजाने संघटितपणे कार्य केले आहे.

या भागातील जैन व्यक्तिमत्त्वांनी केवळ धर्मप्रसारच नव्हे, तर समाजसुधारणा, स्त्री-उन्नती (स्त्री-उद्धार), शिक्षण, आरोग्य, उद्योग, साहित्य, कला, पर्यावरण संरक्षण आणि दानधर्म अशा विविध क्षेत्रांत आपला अमूल्य ठसा उमटवला आहे. अनेक जैन साधू-साध्वी, मुनी, विद्वान, साहित्यिक, उद्योगपती, समाजसेवक, महिला नेत्या आणि तरुण कार्यकर्ते यांनी समाजाच्या आणि पर्यायाने देशाच्या प्रगतीसाठी मोलाचे योगदान दिले आहे. थोडक्यात, दक्षिण महाराष्ट्रातील जैन समाजाचा हा प्रवास म्हणजे परंपरा आणि आधुनिकता, धर्म आणि समाजकारण, स्थानिकता आणि जागतिकता यांचा एक सुंदर संगम आहे. प्रस्तुत शोध निबंधातून आपण या भागातील जैन व्यक्तिमत्त्वे आणि संस्थांच्या योगदानाचा सर्वांगीण आढावा घेणार आहोत.

१. हुतात्मा मोतीचंद :

मोतीचंद यांचा जन्म १८९० साली सोलापूर जिल्ह्यातील करकंब येथे झाला. त्यांना बालपणापासूनच धार्मिक व देशभक्तीचे संस्कार मिळाले. शारीरिक आणि बौद्धिक शिक्षण घेत असतानाच त्यांनी सावरकरांचे जोसेफ मॅझिनी, योगी अरविंदांचे वंदे मातरम् यांसारखी प्रेरणादायक पुस्तके वाचून देशभक्तीची प्रेरणा घेतली. सोलापुरातील देवचंद कस्तुरचंद (नंतरचे मुनिश्री संमतभद्र महाराज) यांच्याशी मैत्री होऊन दोघांनी १९०६ साली 'जैन बालोत्तेजक समाज' या संघटनेची स्थापना केली, ज्याचे उद्घाटन लोकमान्य टिळकांनी केले. मोतीचंदांनी टिळकांच्या राष्ट्रीय विद्यालय स्थापनेसाठी निधी संकलनात मदत केली. पुढे त्यांनी सशस्त्र क्रांतीत भाग घेतला. "राजस्थानमधील निमच गावातील मठाधीशाच्या संपत्तीचा वापर क्रांतीसाठी करण्याचा कट रचण्यात आला, ज्यात मोतीचंद सहभागी होते; या कारवाईनंतर ब्रिटिशांनी शोधमोहीम राबवली, आणि महेंद्रकुमार नाटक प्रकरणाच्या माध्यमातून मोतीचंदांसह अन्य क्रांतीकारकांना अटक झाली. त्यांना खुनासाठी फाशीची शिक्षा झाली."[१] तुरुंगातील त्यांचे आचरण शांत, उदात्त व साधुपणाला साजेसे होते. देशभक्तीबरोबरच त्यांची जैन धर्मनिष्ठाही ठळक होती. मोतीचंद हे एक महान जैन क्रांतीकारक होते ज्यांचे स्वातंत्र्यलढ्यातील योगदान अतुलनीय आहे.

२. आण्णासाहेब लट्ठे:

जैन समाजातील थोर नेते आण्णासाहेब बाबाजी लट्ठे यांचा जन्म ९ डिसेंबर १८७८ रोजी कुरूंदवाड येथे झाला. त्यांनी १८९५ मध्ये मॅट्रीक व १९०१ डेक्कन कॉलेजमधून मुंबई विद्यापीठाची बी. ए. पदवी मिळवली. १९०३ मध्ये उच्च श्रेणीतून एम. ए. पदवी उत्तीर्ण झाले. त्या काळामध्ये एम. ए. होणारे आण्णासाहेब लट्ठे हे जैन समाजातील पहिलेच विद्यार्थी होते. "१८९९ मध्ये वयाच्या एकविसाव्या वर्षी दक्षिण महाराष्ट्र जैन सभा स्थापन करण्यात त्यांचा पुढाकार होता; 'जिनविजय' या मासिकाचे संपादकत्वही सुरवातीच्या काळात त्यांच्याकडे होते."[२]

जैन समाजातील प्रतिष्ठीत जैन व्यक्तींमार्फत त्यांचा कोल्हापूरच्या राजर्षी शाहू छत्रपतींशी निकटचा संपर्क आला. १९११ मध्ये लट्ठेची कोल्हापूर संस्थानाचे विद्याधिकारी म्हणून नेमणूक करण्यात आली. १९१५ मध्ये त्यांनी डेक्कन ब्राह्मणेतर सभेची बेळगावमध्ये स्थापना केली. १९१६ साली पुण्याच्या लॉ कॉलेजमधून एल. एल. बी. झाले. "त्यांनी १९१८ मध्ये 'डेक्कन रयत' हे इंग्रजी साप्ताहिक सुरु केले."[३]

१९२१ ते १९२९ या कालावधीत ते कोल्हापूर संस्थानाच्या विधीमंडळाचे सदस्य होते. १९२४ मध्ये त्यांनी ब्राह्मणेतर काँग्रेसचे अधिवेशन भरविले. "१९२७ साली आण्णासाहेब लट्ठे आणि गांधीजी यांची भेट झाली; १९३० मध्ये संस्थानिकांच्या मार्फत बाजू मांडण्यासाठी इंग्लंडला गोलमेज परिषदेसाठी गेले."[४]

आण्णासाहेब लट्ठे हे ब्रिटीश सरकारने दिलेल्या सर्व पदव्यांचा त्याग करून काँग्रेस पक्षात आले होते. त्या काळात काँग्रेस पक्ष म्हणजे स्वातंत्र्यासाठी लढणारा पक्ष अशी भूमिका असल्याने लट्ठेनी काँग्रेसमध्ये प्रवेश केला होता. "आण्णासाहेव लट्ठेनी स्वातंत्र्यचळवळीत सामान्य स्वातंत्र्यसैनिकाने ज्याप्रमाणे लढा दिला त्याप्रमाणे लढा दिला नसला तरीही संस्थाची राज्ययंत्रणा कार्यक्षमपणे पाहणे, राष्ट्रीय स्वातंत्र्यासाठी जनजागृती करणे यासारखे स्वातंत्र्यचळवळीला पोषक असे कार्य त्यांनी केले."[५]

३. हुतात्मा आण्णासाहेब पत्रावळे :

आण्णासाहेब व्यंकाप्पा पत्रावळे यांचा जन्म १९२५ मध्ये कोल्हापूर जिल्ह्यातील हातकणंगले येथे झाला. १९३८ मध्ये आण्णा सातवी पास झाले होते. शालेय जीवनात हुशार असल्याने त्यांना स्कॉलरशिपही मिळाली होती. लहानपणातच त्यांना देशाच्या स्वातंत्र्यासाठी काहीतरी करावे असे त्यांना वाटू लागले. घरची परिस्थिती चांगली असतांनाही गोरगरिबांना चांगले अन्न खावयास मिळत नाही असे वाटून आण्णा हे साधेच जेवण घेत असत. लहानपणी राष्ट्रीय पुढाऱ्यांची स्फूर्तीदायी चरित्रे व महात्मा

गांधी यांचे हरिजन वृत्तपत्रातील लेख वाचल्यामुळे ते स्वातंत्र्य मिळविण्याच्या भावनेने प्रेरित झाले होते. "१९४२ मध्ये वार्षिक परीक्षा आण्णांनी चांगली दिली पण प्रत्येक उत्तरपत्रिकेत 'गुरुजनहो, नोकरी सोडा, देश स्वतंत्र करण्यासाठी क्रांतीकार्यात भाग घ्या,' असे लिहून ठेवले."[६]

आण्णाच्या वयाच्या अठराव्या व सांगली स्टेशनच्या चौकात स्वातंत्र्यचळवळीच्या प्रचारार्थ सभा चालू होती. या सभेवर पोलीसांनी गोळीबार केला. त्यात अनेक लोक जखमी, घायाळ झाले होते. या लोकांना दवाखान्यात नेण्यासाठी आण्णा हे हिमतीने पुढे गेले. त्याचा पोलीसांना राग आला होता. त्यांनी आण्णांच्या कारवायावर बारकाईने लक्ष ठेवून सांगलीच्या बुरुड गल्लीत बैठक चालू असताना अचानक छापा टाकला, आण्णा पत्रावळेना अटक करून सांगलीच्या जेलमध्ये ठेवण्यात आले. जेलमध्ये आण्णाबरोबर वसंतदादा ही होते. एके दिवशी जेलमध्ये बंद असणाऱ्या सर्व क्रातीकारकांनी तुरुंग फोडून बाहेर पळ काढला पोलीस सर्व क्रांतीकारकांच्या मार्गावर होते. पोलीसांनी क्रांतीकारकांवर गोळ्या झाडल्या. त्यातलीच एक गोळी आण्णांना लागून ते स्वातंत्र्यासाठी हुतात्मे झाले. आजही सांगलीमध्ये आण्णासाहेबांच्या स्वातंत्र्यासाठी दिलेल्या लढ्याची आठवण ठेवण्यासाठी तेथे 'हुतात्मा आण्णासाहेब पत्रावळे चौक' उभारला आहे.

४. भूपाल अणस्कुरे :

भूषाल अणस्कुरे यांचा जन्म १९२७ मध्ये कोल्हापूर जिल्ह्यातील ठिकपुर्ली, ता. राधानगरी या गावी झाला. त्यांचे शिक्षण सहावीपर्यंत झाले. वयाच्या तेराव्या-चौदाव्या वर्षापासून किराणा दुकान चालवून घरच्या परिस्थितीस हातभार लावला. व्यापाराच्या निमित्ताने सांगलीला येणे-जाणे होत असतांना त्यांची स्वातंत्र्यसैनिक पी. बी. पाटील यांच्याशी भेट झाली. त्यांच्या परिचयाने भूपाल अणस्कुरे यांची स्वातंत्र्य लढ्यात सहभाग घेण्याची इच्छा वाढू लागली. त्यांच्या स्वातंत्र्यचळवळीच्या ओढीने त्यांनी लग्न न करता स्वातंत्र्यात सहभाग घेणे अधिक पसंत केले. "भूपाल यांनी १९४२ ची 'भारत छोडो' चळवळ चालू असतांना भूमिगत राहून या चळवळीत कार्य करणाऱ्या स्वातंत्र्यसैनिकांच्या जेवणाची व औषधपाण्याची ते व्यवस्था पाहत; तसेच ते क्रांतीकारकांना बंदुका, बाँब, डायनामाईट या वस्तूही पुरवत."[७]

भूमिगतांना भूपाल यांनी मदत केल्याने ब्रिटीश सरकारने त्यांना अटक केली. तुरुंगात असतांना त्यांचा अनन्वित छळ करण्यात आला. तुरुंगातून सुटण्यासाठी ब्रिटिशांनी त्यांना माफीचा साक्षीदार होण्यास सांगितले पण त्यामुळे आपल्याच सहकाऱ्यांना ब्रिटीश पकडतील हे लक्षात आल्याने त्यांनी माफीचा साक्षीदार होण्यास नकार दिला. कोल्हापूरचे बापूसाहेब मिरजे यांनी पाच हजार रूपयांच्या जामीनावर भूपाल अणस्कुरे यांची सुटका करून आणली. तुरुंगातील अनन्वित छळामुळे भूपाल यांची प्रकृती बिघडली होती. त्यामुळे त्यांच्यावर मिरजेत उपचार सुरू होते. १९४५ मध्ये ब्रिटीशांनी पुन्हा त्यांच्याविरुद्ध खटला भरला. पण त्याच दिवशी त्याचा स्वर्गवास झाला. ब्रिटीश या स्वातंत्र्यप्रेमी देशभक्ताचे काहीही बिघडवू शकले नाही.

५. स्वातंत्र्यवीर सातप्पा :

कोल्हापूर जिल्ह्यातील कडवी शिवापूर या गावी १९१४ मध्ये सातप्पाचा जन्म झाला. सातप्पाचे शिक्षण बेताचेच झाले. गावामध्ये ते शेती करायचे. टिळकयुग संपून गांधीयुगाला सुरुवात झाली होती. १९३० मध्ये गावामध्ये असहकार चळवळीची स्वयंसेवक दले निर्माण झाली होती त्यात त्यांनी सहभाग नोंदविला. या पथकामार्फत त्यांनी आजूबाजूच्या खेड्यामध्ये स्वातंत्र्यप्रेरणा जागृत केली. "१९४० च्या वैयक्तिक सत्याग्रहात सातप्पांनी दोनवेळा सहभाग घेतला; त्यासाठी त्यांना दोनदा हिंडलगा तुरुंगात जावे लागले होते."[८]

गांधीजींचा ऑगस्टचा क्रांतीसंदेश १२ ऑगस्टला शिवापूरात पोहचला. सातप्पांनी चावडीवर तिरंगा फडकावला व गावात सभा आणि मिरवणूक काढली. १५ ऑगस्टला कडवी शिवापूरमध्ये चाळीसे ते पन्नास बंदूकधारी व दहा-पंधरा लाठीधारी पोलीस

गावात आले. साताप्पाच्या नेतृत्वाखाली निघालेली प्रभातफेरी पोलीसांनी थांबवली. पण सातप्पाचा प्रभातफेरी पूर्ण करण्याचा निधार होता. तेव्हा पोलीसांनी प्रभातफेरीतील लोकावर लाठीमार, गोळीबार करण्यास सुरवात केली. सातप्पानी मध्ये राष्ट्रध्वज घेऊन वंदेमातरमच्या घोषणा दिल्या. सातप्पावर पोलीसानी गोळ्या झाडल्या. अखेरच्या क्षणापर्यं सातप्पाचा वंदे मातरम् जयघोष सुरू होता. अशा पद्धतीने सातप्पाने देशासाठी विस्मरण पत्करले.

६. स्वातंत्र्यसैनिक बी. एस. पाटील :

स्वातंत्र्यसैनिक बी. एस. पाटील यांचा जन्म गडहिंग्लज जवळच्या गिजवणे या गावी १८ एप्रिल, १९२७ मध्ये झाला. त्यांचे पूर्ण नाव बाबूराव सातगोंडा पाटील होते. बी. एस. पाटील यांनी शेतीवर स्वयंस्फूर्तीने काम करत आपले शिक्षण घेतले. त्या काळामध्ये देशासाठी लढणाऱ्या माधवराव बागल, रत्नाप्पा कुंभार, दिनकरराव मुद्राळे, पी. बी. पाटील यांचा आदर्श बी. एस. पाटील यांच्या समोर होता. शालेय जीवनातच बी. एस. पाटलांनी खादी वापरायला सुरू करून स्वातंत्र्यलढ्यात उडी घेतली. ८ ऑगस्ट १९४२ मध्ये गांधीजींनी मुंबईच्या गवालिया टंक मैदानावर 'चले जाव'ची हाक देऊन इंग्रजांना भारत सोडून जाण्यास सांगितले. याची माहिती मिळताच १० ऑगस्टला गडहिंग्लजला आल्यानंतर बी. एस. पाटील यांना शाळेतील मित्रांना एकत्र करून गावात भव्य मिरवणूक काढली.

या मिरवणूकीनंतर झालेल्या सभेत बी. एस. पाटील यांनी देशभक्तीने ओथबलेले प्रभावी भाषण केले. बी. एस. पाटील व त्यांच्या समविचारी मित्रांच्या मनात जहाल क्रांतीचे विचार येऊ लागले. बी. एस. पाटील यांच्या पुढाकाराने 'नवजीवन पक्षाची' स्थापना करण्यात आली. या पक्षाने भूमिगत राहून ब्रिटीशांना सळो की पळो करण्याचे धोरण स्वीकारले. त्याचाच एक भाग म्हणून बी. एस. पाटील व त्यांच्या सहकाऱ्यांनी गारगोटी येथील सरकारी कचेरीवर हल्ला करण्याचे निश्चित केले. १३ ऑगस्ट १९४२ मध्ये गारगोटी येथील कचेरीवर हल्ला करण्याचे ठरविण्यात आले. पण तत्पूर्वीच काही क्रांतीकारकांनी कचेरीवर हल्ला केला. पोलीसांच्या गोळीबारात सात क्रांतीकारक मारले गेले. या हल्ल्यासाठी बी. एस. पाटील यांनी क्रांतीकारकांना शस्त्रे पुरविली अशी माहिती पोलीसांना मिळाल्याने त्यांना अटक करण्यासाठी पोलीस त्यांचा शोध घेऊ लागले. बी. एस. पाटील या काळात भूमिगत होऊन कार्य करू लागले. "कोल्हापूरात गावठी बाँबचे प्रयोग करण्यासाठी बी. एस. पाटील येणार असल्याची माहिती पोलीसांना मिळाल्याने बेळगावहून कोल्हापूरला आलेल्या बी. एस. पाटील यांना अटक करण्यात आली."[९]

तुरुंगात त्यांचा अनन्वित छळ करण्यात आला. स्वातंत्र्य चळवळीचा जोर वाढू लागला होता. गांधीजींनी ब्रिटीशांबरोबर वाटाघाटी करून १९४७ पूर्वी सर्व राजकैद्यांना सोडले पाहिजे, अशी अट घाली. त्यामुळे क्रांतीकारकांची ब्रिटीशांनी जेलमधून सुटका केली. त्यात बी. एस. पाटील यांचाही सहभाग होता.

७. माणिकचंद बंडूचंद दोशी :

माणिकचंद यांचा जन्म बंडूचंद व हुलजबाई यांच्या पोटी २८ फेब्रुवारी १९०८ मध्ये झाला. बालवयात त्यांच्यावर जैनधर्माचे व शिवचरित्राचे संस्कार झाले. शिक्षणासाठी सोलापूर येथे आले असतांना रामकृष्ण जाजू, डॉ. आंगोळीकर या देशभक्तांशी त्यांचा संबंध आला. "मुळशीचा सत्याग्रह, जालियनवाला बाग हत्याकांड, महात्मा गांधीचा बहिष्कार कार्यक्रम आणि ॲनी बेझंट यांची व्याख्याने यामुळे ते राष्ट्रकार्यात दाखल झाले.

१९४२ च्या 'भारत छोडो' आंदोलनात त्यांनी खेड्यापाड्यात फिरून जोरदार उठाव घडवून आणला. या मोर्चात सहभागी झालेल्या लोकावर पोलीसानी गोळीबार केला त्यात सहा लोक शहीद झाले. ७ सप्टेंबर १९४२ रोजी सभेला भाषणाद्वारे संबोधीत करत असतांना पोलीसांनी माणिकचंद यांना अटक केली. त्याच्या अटकेमुळे लोकक्षोभ झाला. ठिकठिकाणी अटकेच्या निषेधार्थ हडताळ पाळण्यात आले. सरकारने माणिकचंदाना सातारा येथे एक वर्ष सश्रम कारावास आणि ५० रुपये दंडाची शिक्षा ठोठावली.

तुरुंगामध्ये माणिकचंदानी १२५ ग्रंथ वाचले. रत्नककरंड, श्रावकाचार, गीताई, दि कॅपिटल हे ग्रंथही वाचले. "१९४३ मध्ये तुरुंगातून सुटल्यावर त्यांनी गावोगावी जाऊन राष्ट्रीय सेवादलाचे जाळे विणले; शांततामय सहजीवनासाठी माणिकचंदांनी शांतीसेना शिबिरे घेऊन जनशक्ती संघटीत केली, त्यांच्या कार्यामुळे माणिकचंदांना 'संतश्री' व 'छोटे गांधीजी' ही उपाधी मिळाली."[१०]

८. देशभक्त बाबासाहेब खंजिरे :

यांचा जन्म १९२० मध्ये झाला. यांनी विद्यार्थी दशेपासूनच स्वातंत्र्यलढ्यात सहभाग घेतला. चलेजाव आंदोलनानंतर सरकारी कार्यालयावर हल्ले करण्यास त्यांनी प्रारंभ केला. अनेक रेल्वे स्टेशन जाळून उद्ध्वस्त केली. यामध्ये चंदूर येथील क्रांती सैनिकांनी पुढाकार घेतला होता. या गटाचे नेतृत्व शंकरराव पाटील यांच्याकडे होते. त्यामध्ये कर्नाटकातील काही स्वातंत्र्यसैनिक सामिल झाले होते. त्यांनी हातकणगले स्टेशन उद्ध्वस्त करण्याचा निर्णय घेतला. यामध्ये बाबासाहेब खंजिरे यांचा पुढाकार महत्त्वाचा ठरला. या. स्टेशनच्या संरक्षणासाठी आठ पहारेकरी होते. त्यांना एका गटाने रोखून धरले. काहींनी स्टेशन मास्तरला ताब्यात घेतले, भल्या मोठ्या हातोड्याने घण घालून टेलिग्राफ यंत्र फोडले आणि बरोबर आणलेल्या पत्न्नास डब्यातील रॉकेल शिपडून स्टेशन इमारतीला आग लावली. सर्वत्र अफवा उठली की, पाचशे लोकांच्या तुकडीने स्टेशन जाळले. या घटनेतील सहभागींची नावे पोलीसांनी शोधली. सहा महिने खटला चालला. त्यात २९ आरोपीपैकी २३ जणांना ५ वर्षांची सत्तमजुरी व ५०० रु. दंड ठोठावण्यात आला. यामध्ये बाबासाहेब खंजिरेचा सहभाग होता. "पुढे स्वातंत्र्य मिळाल्यावर इचलकरंजी व सभोवतालची गावे महाराष्ट्रात यावी म्हणून देशभक्त बाबासाहेब खंजिरेंनी मौलिक कार्य केले."[११] ते आमदार असल्याने त्यांचे म्हणणे मान्य करावे लागले. तसेच इचलकरंजी नगरीचा कायापालट घडवून आणण्यासाठी त्यांनी सहकारी चळवळीचा मार्ग स्वीकारला.

९. दादा अप्पाजी बर्डे:

दादा अप्पाजी बर्डे यांनी स्वातंत्र्यचळवळीत महत्त्वपूर्ण कार्य केले. संपूर्ण महाराष्ट्राला 'बर्डे मास्तर' म्हणून परिचित होते. त्यांचा जन्म ३ ऑगस्ट, १९०८ मध्ये इस्लामपूर येथे झाला. सातवीपर्यंतचे शिक्षण पूर्ण करून त्यांनी शिक्षकाची नोकरी पत्करली. ४ एप्रिल १९३० मध्ये नोकरीचा राजीनामा देऊन गांधीजींच्या मिठाच्या सत्याग्रहात सहभागी झाले. २८ मे १९३० रोजी धरासना येथे बर्डे गुरुजी आणि त्यांचे ६५ सहकारी गेले असता ब्रिटिशांनी त्यांना सत्याग्रह थांबवण्याबाबत सांगितलं. त्यावेळी बर्डे गुरुजींनी त्यांना बाणेदार उत्तर दिल 'आम्ही थांबण्यासाठी आलेलो नाही तर मीठ नेण्यासाठी आलो आहोत'. राष्ट्रीय काँग्रेसची सभासद संख्या वाढविणे, ग्रामोद्योग, दारूबंदी, अस्पृश्यता निवारण, स्त्री-शिक्षण इत्यादी कार्य अव्याहतपणे केले. 'चले जाव' आंदोलनातही त्यांनी सक्रीय भूमिका घेतली. "'राष्ट्रसेवा दल' या प्रतिसरकारमधील संस्थेतही त्यांनी तरुणांना प्रशिक्षण देण्याचे महत्त्वाचे कार्य केले."[१२]

निष्कर्ष:

दक्षिण महाराष्ट्रातील जैन समाजाचा इतिहास, त्यातील व्यक्तिमत्त्वांचे कार्य आणि संस्थांचे योगदान हे केवळ या प्रदेशापुरते मर्यादित नसून, महाराष्ट्राच्या आणि देशाच्या सामाजिक-सांस्कृतिक जीवनावरही आपला ठसा उमटवणारे आहे. या प्रकरणाचा सखोल अभ्यास केल्यानंतर हे स्पष्टपणे लक्षात येते की, जैन समाजाने आपल्या मूल्यांवर, परंपरांवर आणि आधुनिकतेच्या स्वीकारावर आधारलेली समाजसेवा, शिक्षण, उद्योग, साहित्य, कला, पर्यावरण, आरोग्य आणि स्त्री-उन्नती अशा विविध क्षेत्रांत मोलाची कामगिरी बजावली आहे.

जैन धर्माच्या अहिंसा, अपरिग्रह, सत्य आणि समता या तत्त्वांचा प्रभाव जैन समाजाच्या प्रत्येक कृतीत दिसून येतो. दक्षिण महाराष्ट्रातील जैन समाजाने या तत्त्वांचा अवलंब करत समाजाच्या सर्वांगीण विकासासाठी आपले जीवन समर्पित केले आहे. जैन

समाजाच्या विविध घटकांनी – कासार, सैतवाल, पंचम, श्वेतांबर, दिगंबर – आपापल्या परंपरेनुसार सामाजिक, धार्मिक आणि सांस्कृतिक क्षेत्रांत महत्त्वपूर्ण योगदान दिले आहे.

शेवटी, दक्षिण महाराष्ट्रातील जैन समाजाचा प्रवास हा परंपरा आणि आधुनिकता, धर्म आणि समाजकारण, स्थानिकता आणि जागतिकता यांचा एक सुंदर संगम आहे. या समाजाने आपल्या कर्तृत्वातून महाराष्ट्राच्या आणि देशाच्या प्रगतीला एक नवी दिशा दिली आहे. भविष्यातही जैन समाजाच्या मूल्यांचा, कार्याचा आणि संस्थांच्या योगदानाचा आदर्श समाजातील इतर घटकांसाठी प्रेरणादायी ठरेल, यात शंका नाही. अशा प्रकारे, दक्षिण महाराष्ट्रातील जैन व्यक्तिमत्त्वे व संस्थांचे योगदान हे समाजाच्या सर्वांगीण विकासासाठी आणि मानवी मूल्यांच्या संवर्धनासाठी अत्यंत महत्त्वाचे आहे. या योगदानाचा अभ्यास केल्याने समाजसेवा, नेतृत्व, धर्म, शिक्षण, उद्योग आणि आधुनिकतेचा संगम कसा साधावा, हे शिकायला मिळते.

संदर्भसाधने:

१. “हुतात्मा मोतीचंद.” प्रगति जिनविजय, अंक ९, शनिवार, २० मे १९५०.

२. देशपांडे, र. स. (१९९७), शिलालेखाच्या डोळ्यांतून महाराष्ट्र, कॉन्टिनेंटल प्रकाशन, पुणे, पृष्ठ क्र. ३४.

३. मेहता हरिशचंद्र (२००४), जैन धर्माचा इतिहास, भारत जैन ग्रंथमाला, मुंबई, पृष्ठ क्र. ८४

४. “आण्णासाहेब लट्ठे.” प्रगति आणि जिनविजय, अंक २३, सोमवार, २८ ऑगस्ट १९५०.

५. प्रगति आणि जिनविजय अंक २३ वा सोमवार २८ ऑगस्ट १९५०

६. मगदूम डी. डी., भारतीय स्वातंत्र्यलढ्यातील जैनांचे योगदान, शरयू दफ्तरी प्रकाशिका, पृष्ठ क्र. ५८.

७. महाराष्ट्राचा स्वातंत्र्य संग्राम -भूपाळ अणस्कुरे, महाराष्ट्र राज्य ग्रंथसंग्रह विभाग, सरकारी मुद्रणालय, मुंबई, १९७७, पृष्ठ क्र.२४५

८. https://www.maharashtraculture.gov.in/freedomfighters/satyappa

९. ‘Freedom Fighter Baburao Satgonda Patil,’ Maharashtra Cultural Affairs Department, accessed January 15, 2023,

https://www.maharashtraculture.gov.in/freedomfighters/bspatil.

१०. माणिकचंद बंडूचंद दोशी, सोलापूर जिल्ह्यातील स्वातंत्र्यसैनिक, संपादक - महाराष्ट्र राज्य संग्रहालय, डायमंड प्रकाशन, पुणे, १९९१, पृष्ठ क्र. ७८.

११. ‘बाबासाहेब खंजिरे,’ शिव-वाणी: अभिवादन स्वातंत्र्यसैनिकांना ध्वनी-मालिका, खंड २२४, राजमती पाटील-बिरनाळे , महाराष्ट्र राज्य साहित्य संस्कृती मंडळ, मुंबई, २००५, पृष्ठ क्र. ४५.

१२. स्वातंत्र्यसैनिक दादा अप्पाजी बर्डे, भारत सरकार संस्कृती मंत्रालय, अंतिम सुधारित १५ मार्च २०२२, https://www.indiaculture.nic.in/freedom-fighters/dada-appaji-barde.